Trehalose recycling promotes energy-efficient biosynthesis of the mycobacterial cell envelope

Amol Arunrao Pohane[a], Caleb R. Carr[a], Jaishree Garhyan[a], Benjamin M. Swarts[b], M. Sloan Siegrist[a,c,*]

[a]Department of Microbiology, University of Massachusetts, Amherst, Massachusetts, USA; [b]Department of Chemistry and Biochemistry, Central Michigan University, Mount Pleasant, Michigan, USA; [c]Molecular and Cellular Biology Graduate Program, University of Massachusetts, Amherst, Massachusetts, USA

Running title: Trehalose recycling supports energy and redox homeostasis

[*]Address correspondence to M. Sloan Siegrist, siegrist@umass.edu

Abstract

The mycomembrane layer of the mycobacterial cell envelope is a barrier to environmental, immune and antibiotic insults. There is considerable evidence of mycomembrane plasticity during infection and in response to host-mimicking stresses. As mycobacteria are resource- and energy-limited under these conditions, it is likely that remodeling has distinct requirements from those of the well-characterized biosynthetic program that operates during unrestricted growth. Unexpectedly, we found that mycomembrane remodeling in nutrient-starved, non-replicating mycobacteria includes synthesis in addition to turnover. Mycomembrane synthesis under these conditions occurs along the cell periphery, in contrast to the polar assembly of actively-growing cells, and both liberates and relies on the non-mammalian disaccharide trehalose. In the absence of trehalose recycling, *de novo* trehalose synthesis fuels mycomembrane remodeling. However mycobacteria experience ATP depletion, enhanced respiration and redox stress, hallmarks of futile cycling and the collateral dysfunction elicited by some bacteriocidal antibiotics. Inefficient energy metabolism compromises the survival of trehalose recycling mutants in macrophages. Our data suggest that trehalose recycling alleviates the energetic burden of mycomembrane remodeling under stress. Cell envelope recycling pathways are emerging targets for sensitizing resource-limited bacterial pathogens to host and antibiotic pressure.

Introduction

The mycobacterial cell envelope is comprised of covalently-bound peptidoglycan, arabinogalactan and mycolic acids, as well as intercalated glycolipids and a thick capsule (1). The mycolic acids attached to the arabinogalactan and the noncovalent glycolipids respectively form the inner and outer leaflets of the mycomembrane, a distinctive outer membrane present in members of the *Corynebacterineae* suborder. The mycomembrane is a key determinant of envelope permeability and home to a variety of immunomodulatory lipids and glycolipids (2-4). There is substantial evidence that the mycomembrane is remodeled *in vivo* and in response to host-mimicking stresses, conditions in which mycobacterial growth and envelope synthesis are presumed to be slow or nonexistent (3, 5-13). While these studies have elucidated bulk changes in mycomembrane composition, the dynamics and subcellular distribution of the molecular transitions have not been characterized. It is also unclear in most cases whether the alterations are solely catabolic, or whether anabolic reactions also contribute to changes in mycomembrane composition under stress.

Recycling pathways are likely to be at the nexus of stress-triggered mycomembrane reorganization. Mycolic acids are ligated to the non-mammalian disaccharide trehalose in the cytoplasm (14). Once transported to the periplasm, trehalose monomycolate (TMM) donates its mycolic acid to arabinogalactan, forming arabinogalactan mycolates (AGM), or to an acceptor TMM, forming trehalose dimycolate (TDM; **Figure 1A**). Both processes release free trehalose. TDM can also be degraded by TDM hydrolase

(TDMH) into TMM and free mycolic acids, the latter of which are an important component of biofilm extracellular matrix in mycobacteria (7, 15). While a salvage mechanism for mycolic acids is still under debate (16-19), recapture of trehalose occurs via the LpqY-SugABC transporter (20). Depending on the specific environmental demand, mycobacteria may funnel reclaimed trehalose back to central carbon metabolism, to generate intermediates for glycolysis or the pentose phosphate pathway, or store it in the cytoplasm, possibly as a stress protectant or compatible solute (6, 21-23). An additional but unexplored potential fate for recaptured trehalose is direct reincorporation into TMM or other glycoconjugates destined for the cell surface. Thus, trehalose connects mycomembrane synthesis and turnover to the metabolic status of the mycobacterial cell.

We find that mycomembrane remodeling triggered by nutrient limitation comprises both synthesis and degradation of AGM and TDM. Remodeling continues in the absence of trehalose recycling. However, compensatory anabolism upsets the energy and redox balance of the cell in a manner indicative of futile cycling (24-28). Similar dysfunction has been proposed to enhance the efficacy of certain antibiotics (29, 30), and indeed, loss of LpqY sensitizes *M. tuberculosis* to multiple drugs (31). Δ*sugC* and Δ*lpqY M. tuberculosis* are also known to be attenuated during infection (20, 32, 33). We show here that inefficient ATP metabolism is the primary mechanism of attenuation in macrophages.

While previous studies identified multiple phenotypes for trehalose recycling mutants, they did not explain how the LpqY-SugABC system contributes to mycobacterial fitness. Our data indicate that trehalose recycling minimizes energy consumption and oxidative stress during mycomembrane adaptation to nutrient limitation. Given the energetic costs associated with *de novo* biosynthesis, recycling pathways for trehalose and other mycomembrane components may be particularly important for *M. tuberculosis* resilience to stress.

Results

Mycomembrane synthesis and degradation are active under carbon limitation. Decreased TDM abundance has been reported for mycobacteria growing in biofilms or adapting to hypoxia or nutrient limitation (3, 5, 7, 23). As uncontrolled TDM hydrolysis results in cell lysis (7, 34), we sought to understand the kinetics of TDM turnover under stress. TMM donates mycolic acids to other molecules of TMM, to form the TDM glycolipid, or to arabinogalactan, to form covalent arabinogalactan mycolates (AGM, **Figure 1A**). The TMM-mimicking probe N-AlkTMM specifically incorporates into TDM because the amide linkage permits mycolic acid acceptance but not donation of the alkyne-appended lipid chain (35). To track TDM hydrolysis under carbon limitation we performed a pulse chase experiment in which we labeled *M. smegmatis* with N-AlkTMM for 12 hours in low (0.02%) glucose-supplemented 7H9 medium, washed, then transferred to 7H9 lacking both the probe and glucose (**Figure 1B, left**). Alkyne-labeled TDM was detected on fixed cells at 0, 4 and 8 hours post-transfer by copper-catalyzed

azide-alkyne cycloaddition (CuAAC) with a fluorescent azide label. We found that TDM labeling decreased by about 3-fold in this time period (**Figure 1B, right**). Fluorescence derived from D-amino acid-labeled cell wall peptidoglycan remained steady, however, consistent with limited bacterial growth under this condition (**Figures 1B, right**, and **Figure S1A**).

Under acid stress, non-replicating but metabolically-active *M. tuberculosis* make new TDM (9). We found that N-AlkTMM uptake (no chase) increased approximately two-fold in low glucose medium (**Figure 1C**). However, a decline in the steady-state abundance of TDM (**Figures 1D, S2B**) suggested that enhanced synthesis is outweighed by the TDM turnover observed in the pulse-chase experiment (**Figure 1B, right**).

We wondered whether there might be additional changes in mycomembrane metabolism. O-AlkTMM is also a TMM-mimicking probe but features an ester-linked lipid chain. While the molecule can serve as either an alkyne-lipid donor or acceptor, ~90% of labeling from this probe is present in the *M. smegmatis* AGM cellular fraction (35). O-AlkTMM uptake was enhanced in low glucose medium to a greater extent than N-AlkTMM (**Figure 1C**). The fluorescence signal derived from this probe was also more persistent than N-AlkTMM in a no probe, no glucose chase (**Figure 1B**).

A variety of carbohydrates can serve as mycolate acceptors, including glucose (36, 37). High levels of glucose in the growth medium might therefore suppress O-AlkTMM labeling of the cell surface by competing with arabinogalactan. While in our labeling

window *M. smegmatis* grew faster in 7H9 medium with high (2%) vs. medium (0.2%) glucose supplementation, O-AlkTMM-derived fluorescence in the high glucose condition was lower (**Figure S1B**). However, O-AlkTMM labeling was similar for *M. smegmatis* in 0.2% or 0.02% glucose or acetate (**Figure S1B**), despite sluggish or absent bacterial replication under the low carbon conditions (**Figure S1A**). Thus, incorporation of O-AlkTMM into AGM is suppressed in high glucose, likely because the alkyne-fatty acid from the probe is transferred to the unanchored glucose and washed away. Nonetheless our data indicate that substantial AGM synthesis occurs in growth-limiting amounts of glucose or acetate. As the steady-state abundance of the molecule did not change in carbon-limited medium (**Figure 1D, S2C**), these experiments also suggest that AGM synthesis is balanced by the turnover that we observed by pulse-chase (**Figure 1B, right**).

We previously showed that the fluorescent D-amino acid HADA and alkDala incorporate into *M. smegmatis* peptidoglycan via both cytoplasmic and L,D-transpeptidase enzymes (38). HADA and alkDala labeling roughly correlated with mycobacterial growth rate under different amounts of glucose or acetate (**Figures 1C, S1A, S1C**). Suppressed levels of peptidoglycan synthesis or remodeling during carbon limitation stood in contrast to active mycomembrane metabolism.

AGM synthesis occurs along the periphery of the mycobacterial cell during carbon limitation. TDM hydrolysis enhances envelope permeability in oleic acid- and glucose-deprived *M. tuberculosis* (3). Surprisingly, despite an analogous decrease in

TDM abundance (**Figures 1D, S2B**), *M. smegmatis* became less permeable to propidium iodide when cultured in glucose-limited medium (**Figure 1E**). Global AGM levels have also been linked to mycobacterial permeability (39). While AGM abundance was relatively unaffected in glucose-deprived medium (**Figures 1D, S2C**), our data suggest that the apparent stasis belies active synthesis and degradation (**Figures 1B, 1C**). We wondered whether AGM remodeling might impact its spatial distribution, which in turn could alter cell permeability.

Mycobacteria growing in nutrient-replete medium construct their cell envelope in gradients that emanate from the poles and continue along the sidewall (35, 38, 40-48). While polar peptidoglycan synthesis promotes cell elongation, sidewall synthesis occurs in response to cell wall damage (49). We hypothesized that the AGM synthesis that we observe under carbon deprivation (**Figure 1C**) is a cell-wide response, similar to peptidoglycan repair. Quantitative fluorescence microscopy revealed that O-AlkTMM labeling of *M. smegmatis* growing in carbon-replete medium comprised polar gradients (**Figure 1F**) as expected (35, 38). However, in slow or non-growing, carbon-deprived *M. smegmatis*, O-AlkTMM-labeled species were more evenly distributed around the periphery of the cell. This observation suggests that AGM synthesis fortifies the mycomembrane along the sidewall as mycobacteria adapt to carbon deprivation.

Trehalose cycling supports mycomembrane metabolism during carbon starvation. Mycomembrane synthesis centers on the mycolic acid donor trehalose monomycolate (TMM). Prior to its export to the periplasm, TMM is synthesized in the

cytoplasm by the ligation of a mycolic acid to trehalose (50). *De novo* synthesis of mycolic acids and trehalose is both energy- and resource-intensive; recycling pathways for both molecules have been shown or proposed (18-20). We hypothesized that nutrient-starved mycobacteria might buffer the costs of TMM synthesis by enlisting recycling pathways. As the recycling mechanism for mycolic acids is still controversial (16, 17), we focused on the role of trehalose uptake.

Trehalose released as a byproduct of extracellular mycomembrane metabolism is recycled via the LpqY-SugABC transporter ((20), **Figure 2A**). At least two different processes liberate trehalose: ligation of mycolic acids from TMM to arabinogalactan to form AGM and transfer of mycolic acids from TMM to another molecule of TMM to form TDM (**Figure 1A**). Breakdown of TDM by the TDM hydrolase (TDMH) yields TMM and mycolic acids (7, 15, 34), so subsequent use of TMM in the forgoing reactions would also release trehalose. Our metabolic labeling results suggested that all of these processes are active as *M. smegmatis* adapts to carbon limitation (**Figure 1**). We were unable to measure extracellular trehalose levels in wild-type *M. smegmatis*, presumably because LpqY-SugABC rapidly internalizes the disaccharide (20). However by using Δ*sugC M. smegmatis*, a strain that lacks a functional trehalose transporter, we were able to detect elevated levels of trehalose in the supernatant when bacteria were grown in carbon-limited conditions (**Figure 1G**; note that we used glycerol as the carbon source as glucose interferes with the assay). We also found that free mycolic acids accumulated in the supernatant of low glucose cultures (**Figure 1D, S2D**), as expected

from TDM turnover. Together our data indicate that trehalose is liberated upon reorganization of the mycomembrane.

Exogenously-supplied trehalose can support mycobacterial growth (20) after it is transported by LpqY-SugABC (20) and metabolized by trehalase (21) or TreS (6, 50-52) (**Figure 2A**). We recovered similar colony-forming units (CFU) for Δ*sugC*, Δ*tre*, Δ*treS* and wild-type *M. smegmatis* from 1, 2, 4 and 6 days in low glucose (**Figures 2B, 2C**). These data suggest that trehalose catabolism is not required for viability, nor does it fuel appreciable cell growth, under carbon deprivation. Given that both the optical density and colony-forming units of *M. smegmatis* were steady (**Figures 2B, 2C, S1A**), trehalose recovered from the mycomembrane also does not fuel appreciable cell growth under this condition.

In hypoxic and biofilm cultures of *M. tuberculosis*, TMM and TDM levels decrease (5, 6, 23). Glycolipid turnover occurs rapidly in the former, within 4 hours (6), and slowly in the latter, within 16 days (23). We did not observe a net decrease in TMM for *M. smegmatis* or *M. tuberculosis* under carbon limitation (**Figures 2F, 2G**) despite an increase in TMM-consuming AGM and TDM remodeling (**Figure 1C**). We posited that TMM pools might be replenished by recycled trehalose. Metabolic incorporation of exogenous 6-azido-trehalose (6-TreAz) by *M. smegmatis* or *M. bovis* BCG requires uptake by LpqY-SugABC (53). We found that 6-TreAz labeling was enhanced in slow-growing, glucose-starved *M. smegmatis* (**Figure 2D**) or oleic acid- and glucose-starved *M. tuberculosis*

(**Figure 2E**, (3)). As incorporation of the metabolite was respectively abolished or diminished in Δ*sugC M. smegmatis* (**Figures 2D** and **S3A** (53)) or *M. tuberculosis* (**Figure 2E**), enhanced 6-TreAz labeling under carbon limitation indicates an increase in trehalose recycling.

6-TreAz recovered by the LpqY-SugABC transporter may remain intact in the cytoplasm, be catabolized, or be converted to azido-TMM and transported outside of the cell (**Figure 2A**, (53)). Although it has not been reported, it is possible that the probe incorporates into other trehalose-bearing molecules in the mycobacterial envelope (21). To tune our detection for the cell surface, we selected DBCO-Cy5 as the fluorescent, azide-reactive label because the localized charge on the sulfonated cyanine dye confers poor membrane permeability (54). The enhanced 6-TreAz labeling that we observed for *M. smegmatis* and *M. tuberculosis* during carbon limitation (**Figures 2D, 2E**) strongly suggests that at least some of the recycled trehalose is converted into an envelope component(s). Given that 1) TMM and TDM are the only known trehalose-containing glycoconjugates shared by both *M. smegmatis* and *M. tuberculosis*, and that 2) TDM cannot be labeled by 6-TreAz (53), we conclude that TMM is the most likely target. As steady-state TMM levels remained relatively constant in both species (**Figures 2F, 2G, S3B, S3C**), enhanced conversion of 6-TreAz to azido-TMM further suggests that trehalose recycling under carbon deprivation helps to maintain TMM levels. These data are consistent with a model in which trehalose cycles in and out of the cell to remodel the mycomembrane in carbon-deprived mycobacteria.

Mycomembrane reorganization under carbon deprivation can occur in the absence of trehalose cycling. Our experiments suggest that trehalose cycling contributes to mycomembrane reorganization during carbon limitation. However, loss of trehalose import by LpqY-SugABC did not impact the abundance of TMM, TDM or AGM (**Figures S2B, S2C, S3B, S3C, S4B, S4C**); synthesis of AGM or TDM (**Figure S4D**); turnover of TDM (compare **Figure 1B, right**, to **Figure S4E**); or permeability (**Figure S4F**). The absence of measurable changes in mycomembrane metabolism or composition were consistent with earlier work showing that Δ*sugC* and Δ*lpqY M. tuberculosis* do not have detectable changes in the glycolipid composition of their mycomembrane compared to wild-type (20). These data also indicate that mycomembrane reorganization can occur in the absence of trehalose recycling.

Trehalose recycling promotes redox and energy homeostasis under carbon limitation. While trehalose recycling was dispensable for *M. smegmatis* and *M. tuberculosis* mycomembrane remodeling and survival under carbon limitation, we hypothesized that it might be important for withstanding other stressors. We first asked whether blocking trehalose recycling disrupts redox homeostasis. We tested this hypothesis under growth-limiting (**Figure S1**, (3)) carbon limitation as trehalose recycling is enhanced in this condition (**Figures 2D, 2E**).

Δ*sugC M. smegmatis* and *M. tuberculosis* were sensitized to exogenously-applied hydrogen peroxide and/or to ROS-potentiating vitamin C (55), (**Figures 3A, 3B, S5A**

and **S5B**). Loss of trehalose recycling also enhanced the fluorescence of dihydroethidium (DHE), an indicator dye of endogenous cellular superoxide (**Figure 3C**, (56)). Propidium iodide staining remained unchanged (**Figure S4F**), suggesting that the effect was not due to nonspecific differences in uptake, efflux or cell size. In *M. smegmatis*, the total pool of cytoplasmic thiol antioxidants was modestly enhanced in the absence of *sugC* (**Figure S5C**). We hypothesized that the increase in free thiols in the *sugC* mutant might be an adaptation to counteract the higher basal levels of superoxide. Consistent with a drive to maintain a reduced thiol pool (57) (58), we observed increased NADP:NADPH (**Figure S5D**) in Δ*sugC M. smegmatis.* Taken together, our data suggest that trehalose recycling that occurs during carbon limitation supports redox balance.

A possible endogenous source of ROS in the bacterial cell is respiration, which in turn can be estimated by the oxidation of the methylene blue dye (59). In carbon-limited medium, we observed more methylene blue decolorization for Δ*sugC* (**Figure 3D**), indicating that respiration is enhanced in the absence of trehalose recycling. Notably, however, the mutant had lower levels of ATP than wild-type (**Figure 3E**). These data are consistent with a model in which trehalose recycling maintains redox balance in carbon-limited mycobacteria by minimizing ATP consumption and respiration (**Figure 3F**). Alternatively, or additionally, redox balance may enable energy homeostasis under this condition.

Trehalose anabolism disrupts redox balance under carbon limitation. Cytoplasmic trehalose can protect against ROS directly, in plants, fungi and other bacteria (60-63), or indirectly, via TreS-dependent catabolism in mature *M. tuberculosis* biofilms (23). To test whether either of these potential mechanisms could account for recycling-promoted redox homeostasis, we measured the total trehalose pools, endogenous ROS levels, and exogenous ROS sensitivity of mutants defective in trehalose catabolism or anabolism. There are several metabolic pathways for trehalose in mycobacteria: OtsA and OtsB convert phosphorylated glucose intermediates to trehalose; TreY and TreZ degrade the glucose polymer α-glucan into trehalose; TreS converts trehalose to maltose; trehalase degrades trehalose into glucose (**Figures 2A** and **S6A**). We found that changes to the size of the trehalose pool that were due to perturbations in catabolism (**Figures S6G** and **S6H**) or anabolism (**Figure S6B**) did not correlate with endogenous ROS levels (**Figure S6C**) or sensitivity to exogenous ROS (**Figures S6D, S6E** and **S6F**). These experiments indicated that the mycobacterial redox balance does not depend solely on the size of the trehalose pool nor on trehalose catabolism during short-term carbon limitation.

How might trehalose recycling promote redox homeostasis under nutrient limitation? We noted that mycomembrane synthesis continues unabated in Δ*sugC* (**Figure S4D**) and that TMM remains at wild-type levels (**Figures 2F** and **2G**). The synthetic lethal interactions between *otsA* and *treYZ* or *lpqY-sugABC* in *M. tuberculosis* (64) suggest functional redundancy between the pathways encoded by these genes. The TreYZ pathway does not require energy to break down α-glucan into trehalose but OtsA and

OtsB convert phosphorylated glucose intermediates to trehalose. In glucose-limited conditions, trehalose biosynthesis via the OtsAB pathway may also require additional ATP to drive gluconeogenesis. We wondered whether induction of ATP-expensive trehalose anabolism might explain the oxidative stress that occurs in the absence of LpqY-SugABC.

Four lines of evidence support the first part of this model. First, Δ*sugC M. smegmatis* consume more ATP than wild-type (**Figure 3E**). Second, we observed enhanced metabolism of fluorescently-labeled glucose in the mutant (**Figure S7**). Third, while expression of *otsA* did not change and expression of one of the two *M. smegmatis otsB* homologs, (MSMEG_6043) was not detectable, expression of the other *otsB* homolog, MSMEG_3954, was enhanced ~4-fold in the absence of *sugC* (**Figure 4A**). Finally, the levels of glucose-6-phosphate—the end product of gluconeogenesis—were elevated in Δ*sugC* but suppressed in Δ*otsA* (**Figure 4B**), respectively consistent with increased and decreased flux through this pathway.

We next tested the second part of our model *e.g.* whether induction of trehalose anabolism upsets redox balance in carbon-deprived mycobacteria. Given the synthetic lethal interaction between *sugC* and *otsA* (64), we opted to deplete the trehalose pool by inducible trehalase overexpression. We compared the hydrogen peroxide sensitivity of strains that overexpress trehalase in wild-type, Δ*otsA* and Δ*treYZ* backgrounds. Loss of OtsA, but not TreYZ, rescued sensitivity of *M. smegmatis* to hydrogen peroxide upon

trehalase overexpression (**Figure 4C**). These experiments indicate that trehalose replenishment by the OtsAB pathway can sensitize carbon-starved mycobacteria to ROS. Taken together, our data suggest that trehalose recycling limits energy consumption and oxidative stress during carbon limitation by alleviating the need for *de novo* biosynthesis.

Trehalose recycling promotes *M. tuberculosis* survival in macrophages. Deletion of *sugC* or *lpqY* inhibits *M. tuberculosis* replication in the acute phase of murine infection (20). Transposon insertions in *sugABC or lpqY* also attenuate pooled *M. tuberculosis* growth in IFN-γ-activated or resting C57BL/6 bone marrow-derived macrophages (BMDMs; (32)). While it is likely that progressive carbon starvation underlies the *in vivo* and macrophage defects of trehalose recycling mutants, the precise mechanism(s) have not been clear. Our *in vitro* experiments support a model in which trehalose anabolism compensates for the loss of trehalose recycling but exacts energetic and redox costs. Since one consequence of IFN-γ activation is ROS production by the macrophage (65, 66) we first sought to test whether the magnitude of trehalose recycling mutant attenuation was different in the presence or absence of the cytokine. We confirmed that Δ*sugC M. tuberculosis* was defective for growing in immortalized BMDM and that this phenotype was reversed by genetic complementation (**Figures 5A, 5B**). However the IFN-γ-dependent decrease in Δ*sugC* fitness relative to wild-type was very modest (**Figure S8A**), suggesting that sensitivity to ROS or to other, downstream stresses like reactive nitrogen intermediates, acidic pH and nutrient limitation (67, 68) does not fully account for attenuation in macrophages.

We next asked whether dysfunctional energy metabolism compromises the fitness of trehalose recycling mutants during infection. To do this, we took a chemical-genetic epistasis approach. Bedaquiline inhibits ATP production by targeting the F_1F_0 ATP synthase (69, 70). Bedaquiline-treated *M. tuberculosis* is transiently able to maintain ATP levels by increasing oxidative and substrate-level phosphorylation (71, 72). Loss of trehalose recycling also results in ATP depletion (**Figure 3E**) and enhanced respiration (**Figure 3D**) *in vitro*. If these perturbations to (energy) metabolism are responsible for trehalose recycling mutant attenuation, we reasoned that bedaquiline should inhibit wild-type and Δ*lpqY* or Δ*sugC M. tuberculosis* similarly *e.g.* that the drug should not be additive with either of the mutations. Indeed we found that loss of *lpqY* or *sugC* was additive with treatment with rifampicin, an antibiotic that does not impair mycobacterial energy metabolism (73, 74), but not with bedaquiline (**Figure 5C, S8B**). Taken together our data suggest that energy dysfunction that accompanies loss of trehalose recycling attenuates *M. tuberculosis* in macrophages.

.

Discussion

Hints of mycomembrane plasticity began to appear in the early 1900s, when it was recognized that acid-fastness–a hallmark staining property still used for microscopy-based diagnosis of *M. tuberculosis*—varied with nutrient supply (75-77). More recent work supports the idea that the mycomembrane is reconfigured *in vivo* and in response

to host-mimicking stresses (3, 5-13). The mechanisms by which these cell surface alterations occur are still emerging but have been attributed primarily to catabolic pathways (3, 6). We took advantage of recent advances in metabolic labeling (35, 78) to show that mycomembrane remodeling under *in vitro* carbon deprivation also involves anabolic reactions (**Figure 1C**), a counterintuitive result as mycobacterial replication (**Figure S1A**) and presumably overall metabolic activity are sluggish. Our data collectively indicate that the net result of such reactions is decreased TDM and spatial rearrangement of AGM. We previously showed that synthesis of peptidoglycan along the non-expanding sidewall of *M. smegmatis* is enhanced in response to cell wall damage (38). AGM synthesis under carbon starvation also occurs along the cell periphery (**Figure 1F**), further supporting the notion that mycobacteria can edit their cell surface in a growth-independent fashion.

The adaptive consequences of mycomembrane remodeling are manifold (21, 79, 80). For example, bulk decreases in TDM and AGM abundance are known to increase mycobacterial cell permeability, which in turn enhances nutrient uptake and antimicrobial susceptibility (3, 4, 39). Although we do not observe gross changes in the amount of AGM under nutrient deprivation (**Figure 1D**), the primary site of synthesis shifts from the pole to sidewall (**Figure 1F**). The concomitant reduction in permeability (**Figure 1E**)—despite an overall decrease in TDM abundance—suggests that the subcellular distribution of AGM also contributes to the barrier function of the mycobacterial cell envelope. Beyond enabling edits to the structural components of the mycomembrane, remodeling reactions liberate smaller molecules that influence cell

physiology. Free trehalose released by TDM and AGM synthesis can be recycled into glycolysis or pentose phosphate intermediates, or act as a stress protectant or compatible solute in the cytoplasm (6, 21-23). Our data suggest that it can also be directly refashioned into trehalose-containing, cell surface glycolipids (**Figures 2D, 2E**), likely TMM. Free mycolic acids generated by TDM hydrolysis are components of biofilm matrix (7) and, like trehalose, serve as carbon sources (81). We speculate that they may additionally be reused together with recycled trehalose to make TMM.

How do mycobacteria power mycomembrane remodeling when faced with a loss of nutrients? The three isoforms of the TMM-consuming Antigen 85 complex, encoded in *M. tuberculosis* by *fbpA, fbpB* and *fbpC*, have partially redundant acceptor specificities (39, 82). However only *fbpC* is upregulated in nutrient-starved *M. tuberculosis* (83, 84) making Ag85C an obvious candidate for performing synthetic reactions under that condition. Perhaps the more interesting question, however, is the source of the energetically-expensive TMM building blocks. Breakdown of TDM by TDMH furnishes free mycolic acids and TMM, the latter of which could serve as a donor for sidewall AGM synthesis (7, 15). While such a pathway would not require ATP, it would be limited by the amount of TDM loss that can be tolerated without lysis (7, 34) or reduced resilience to host stress (3). Our data suggest that *M. smegmatis* and *M. tuberculosis* also generate TMM in the cytoplasm from recycled trehalose (**Figures 2D, 2E**). An intracellular route of TMM generation would limit TDM loss, thereby preserving mycomembrane integrity. Use of recycled materials in turn would allow the mycobacterial cell to reap the benefits of sidewall AGM fortification while minimizing

energy expenditure. In the absence of trehalose recycling, *de novo* synthesis supplies the sugar and mycomembrane remodeling continues unabated (**Figure S4**). The cost of from-scratch, OtsAB-mediated anabolism is not apparent under standard *in vitro* culture conditions but sensitizes *M. smegmatis* and *M. tuberculosis* to ROS (**Figure 3**) and may contribute to defective *M. tuberculosis* growth during infection (**Figure 5,** (20)).

Trehalose is a cytoplasmic stress protectant and compatible solute and, in many types of bacteria, a carbon source (62, 85, 86). Mycobacteria and related organisms are relatively unique in using trehalose for extracellular purposes, to build their outer cell envelope. As the sugar fluxes in and out of central metabolism and the mycomembrane via several synthetic (OtsAB, TreYZ) and degradative (TreS, trehalase) processes, trehalose utilization may be particularly vulnerable to perturbations that induce redox and metabolic imbalances. Like carbon-limited Δ*sugC M. smegmatis* or *M. tuberculosis*, biofilm cultures of Δ*treS M. tuberculosis* have disruptions in energy and redox homeostasis (23). However, our data suggest that the mechanisms are distinct. In mature biofilms, trehalose is shunted away from TMM and TDM synthesis into glycolytic and pentose phosphate intermediates in a TreS-dependent manner (23). By contrast, we find that TMM levels are maintained during the time frame of our experiment, either by LpqY-SugABC, in wild-type organisms, or by *de novo* synthesis, in Δ*sugC* mutants. While biofilm Δ*treS M. tuberculosis* are likely more sensitive to ROS because they are depleted for the antioxidant precursor γ-glutamylcysteine (23), carbon-limited Δ*sugC M. smegmatis* have higher levels of ROS-counteracting, cytoplasmic thiols (**Figures S5C**). Finally, biofilm Δ*treS M. tuberculosis* is hyper-sensitive to ATP-depleting bedaquiline

(23) whereas intracellular Δ*sugC* and Δ*lpqY* are more tolerant (**Figure 5C**). These and other metabolite data are most consistent with the idea that enhanced ROS production and susceptibility (**Figure 3**) in the absence of trehalose recycling stems from increased anabolism of the sugar rather than decreased catabolism. While we focus here on mycomembrane remodeling that occurs within 1-3 days of adaptation to carbon-limited medium, the TreS-dependent, trehalose-catalytic shift occurs in 4-5-week-old biofilms. Under our conditions, loss of TreS has no impact on ROS susceptibility (**Figure S6E**). While we cannot rule out stress- or species-specific differences between the two studies, we favor a model in which the adaptive role of trehalose changes over time: early fortification of the cell envelope, to protect against immediate environmental insults, and later rewiring of central carbon metabolism, to maintain ATP and antioxidant levels. Trehalose recycling maintains redox and ATP homeostasis in the second case by driving glycolysis and the pentose phosphate pathway, and in the first case by providing energetically-inexpensive substrates for mycomembrane remodeling, thereby easing the demand for the products of these metabolic pathways.

The presence of a retrograde transporter enables trehalose to cycle in and out of the cell and serve as a metabolic node between the mycomembrane and cytoplasm. Recycling of the sugar is known to enhance *M. tuberculosis* survival in a mouse model of tuberculosis. It is widely hypothesized that the *in vivo* growth defects of trehalose recycling mutants stem from progressive carbon starvation (20, 21, 50). Nutrient deprivation coupled with loss of trehalose catabolism may indeed reduce fitness *in vivo*. However, our data suggest a more complex model, namely that futile trehalose cycling

consumes ATP and stimulates compensatory, ROS-generating respiration (**Figure 6**). The energy and redox phenotypes of a trehalose recycling mutant resemble those elicited by other futile cycles (24-28) and some bacteriocidal antibiotics (29, 71, 72, 87, 88). Enhanced bacterial respiration has been proposed to increase drug efficacy (29, 30), and indeed, loss of trehalose recycling sensitizes *M. tuberculosis* to multiple antibiotics (31). Here we found that disrupted energy metabolism is the primary mechanism of attenuation for trehalose recycling mutant *M. tuberculosis* in macrophages (**Figure 5**). Dysfunction triggered by forced *de novo* synthesis of energy-expensive macromolecules may be a fruitful avenue for potentiating both immune and antibiotic activity against bacterial pathogens, including those that inhabit growth-limiting, nutrient-deprived host niches.

Materials and Methods

Bacterial strains and culture conditions. *M. smegmatis* mc^2155 was grown in Middlebrook 7H9 growth medium (HiMedia, India) supplemented with Tween-80 (7H9T) and glucose (2% or 0.02%) at 37°C unless otherwise specified in the text. Two day-old primary cultures of *M. smegmatis* grown in 2% glucose were normalized to an OD_{600} of 0.1 in fresh 7H9T supplemented with 2% or 0.02% glucose and allowed to grow for 24 hours. *M. tuberculosis* H37Rv strains (gifts of Dr. Rainier Kalscheuer) were grown in Middlebrook 7H9 medium (BD Difco, Franklin Lakes, NJ) supplemented with Tween-80 and OADC (BD BBL, Sparks, MD). For starvation of *M. tuberculosis*, cultures grown in

7H9T-OADC to OD_{600} 0.8-1.0 were collected by centrifugation and washed once with 7H9T (no OADC) and resuspended in 7H9T (starvation medium) to a normalized OD_{600} of 1. To prepare a strain that expresses *tre*, the gene that encodes trehalase, under an acetamide-inducible promoter, we PCR amplified *tre* from genomic DNA of *M. smegmatis* by using 4535For_Acet (tgatgtgctctagagttctgcaacagaccgagcc) and 4535Rev_Acet (ggcctgatctagacatcggggcgttcgcgg) primers. The resulting PCR product was ligated in pYAB033 vector (gift of Dr. Yasu Morita) at XbaI site and transformed in *E. coli* XL-1 blue strain. The colonies were screened by colony PCR and the obtained plasmid was sequence-confirmed. Bacteria used in this study are listed in **Table 1.**

ROS sensitivity. *M. smegmatis* grown in 0.02% glucose for 24 hours were normalized to OD_{600} of 1. The cultures were then treated with 0.15% H_2O_2 for 10 minutes at 37°C with shaking. The trehalase overexpression strains were grown for 20 hours in 0.02% glucose and then induced with 0.2% acetamide for an additional 10 hours before being treated with 0.1% H_2O_2 for 10 minutes at 37°C with shaking. After H_2O_2 treatment, 3 µL of 10-fold serial dilutions made in PBS was spotted on 7H9-2% glucose agar. For thiourea rescue experiment, cultures were pretreated with 50 mM thiourea for 45 minutes prior to H_2O_2. For *M. tuberculosis*, cultures in starvation medium were grown for 5 days, normalized to OD_{600} 0.1 in fresh starvation medium then treated with 0.4% of H_2O_2 for 2 hours at 37°C with shaking. After H_2O_2 treatment, 5 µL of 10-fold serial dilutions made in PBS were spotted on 7H10-OADC agar plate. For the vitamin C experiment, *M. tuberculosis* cultures in starvation medium were normalized to OD_{600} 0.1 in fresh starvation medium. The cultures were then treated with 20 mM vitamin C for 2

days. After vitamin C treatment, 5 µL of 10-fold serial dilutions made in PBS were spotted on 7H10-OADC agar.

Macrophage infections. Immortalized C57BL/6 bone marrow-derived macrophages (iBMDM, gift of Dr. Christopher Sassetti) were seeded at 10^5 cells/well in 24-well tissue culture plate and incubated at 37°C overnight. *M. tuberculosis* were added at 5:1 0-5of infection (MOI; bacteria:iBMDM) and incubated for 4 hours. After incubation the co-culture was washed twice with high glucose Dulbecco's modified Eagle's medium (DMEM, Genesee Scientific, San Diego, CA), to remove extracellular *M. tuberculosis,* and fresh DMEM-FBS-HEPES (5 mM) medium was added (FBS, Genesee Scientific, San Diego, CA and HEPES; Gibco, Paisley, PA, UK). IFN-γ (PeproTech, Rocky Hill, NJ) was added or not at 25 ng/mL concentration. For antibiotic susceptibility experiments, co-cultures were treated or not with 5 µg/mL of bedaquiline (BDQ) or rifampicin (RIF) for two days of the infection. The infected iBMDM were incubated for 0-5 days, then washed once with PBS and lysed with 0.05% Triton-X 100 in PBS. After lysis, 10 µL or 50 µL of 10-fold serial dilutions made in PBS were respectively spotted or spread on 7H10-OADC agar for determining colony-forming units (CFU).

Bliss scoring. Bliss interaction scores (89) for pairs of mutant-drug interactions were obtained by subtracting the expected values for inhibition from the observed values. The expected values were calculated using the formula $E_M+E_A-E_ME_A$ where E_M is the effect of the mutation (Δ*sugC* or Δ*lpqY*) and E_A is the effect of antibiotic (bedaquiline or

rifampicin). Statistically-significant combinations that produced Bliss scores ≠ 0 were interpreted as non-additive interactions.

DHE staining. *M. smegmatis* grown for 24 hours in 7H9T-0.02% glucose were normalized to OD_{600} 1 with the same medium then treated with 5 μM dihydroethidium (DHE; Sigma, St. Louis, MO) for 30 minutes at 37°C. Fluorescence was analyzed by flow cytometry.

Total thiol abundance. The protocol for measuring the total thiol content was adopted from (30). Briefly, 10 mL of *M. smegmatis* grown for 24 hours in 7H9T-0.02% glucose were centrifuged at 2500xg for 5 minutes, washed with buffer containing 50 mM Tris-Cl (pH 8) and 5 mM EDTA, and cell pellets were normalized by wet weight. Bacteria were resuspended in the same buffer and lysed by bead beating. Lysates were centrifuged at 16000xg for 15 minutes at 4°C and 5,5′-dithiobis (2-nitrobenzoic acid) was added to 100 μL of supernatants to a final concentration of 0.05 mM. Total thiol content was estimated by absorbance at λ412nm.

Methylene blue. *M. smegmatis* grown for 24 hours in 7H9T-0.02% glucose were adjusted to OD_{600} 0.25. Cultures were split in two, one of which was treated with 0.005% methylene blue, then aliquoted to a 96-well plate. The plate was sealed with Microseal 'B' Adhesive Sealing Films (BioRad, UK) and incubated at 37°C for 4 hours

with shaking. The seal was then removed and absorbance at λ665nm was measured. The difference between the λ665nm of treated and untreated samples was plotted.

ATP, glucose-6-phosphate and NADP/NADPH quantitation. ATP concentration was measured by by BacTiter-Glo (Promega, Madison, WI) luminescence kit. Glucose-6-phosphate (G6P) concentration and NADP/NADPH ratio were respectively measured with the Amplite™ (AAT Bioquest, Sunnyvale, CA) Colorimetric G6P Assay and Colorimetric NADP/NADPH Ratio Assay kits. *M. smegmatis* grown for 24 hours in 7H9T-0.02% glucose was washed once with PBS. The pellets were resuspended in PBS and lysed by bead beating. Lysates were normalized by total protein concentration using a BCA protein assay kit (Pierce, Rockford, IL) then processed according to the manufacturer's protocol.

Trehalose quantitation. For intracellular trehalose detection, *M. smegmatis* grown for 24 hours in 7H9T-0.02% glucose were washed once with PBS. Cell pellets were normalized by wet weight then resuspended in chloroform:methanol (1:1) for overnight incubation with shaking. The suspension was centrifuged at 10000xg for 5 minutes and the organic fraction was collected in a new tube. One part chloroform and one part water were added to the organic fraction and mixed vigorously in shaker for 15 minutes. Suspensions were centrifuged and the upper aqueous layers were processed per the manufacturer's instructions for the trehalose assay kit (Megazyme, Ireland). For extracellular trehalose detection, *M. smegmatis were* grown for 24 hours in 7H9T

supplemented with 2% or 0.02% glycerol. Cultures were normalized to OD_{600} 1 prior to centrifugation. The upper layer was collected and filtered through a 0.2 µM syringe. Filtrates were processed as above to detect trehalose.

Lipid extraction and TLC. For extractable lipid analysis, 10 mL of culture was washed with PBS and cell pellets were normalized by wet weight (*M. smegmatis*) or by OD_{600} (*M. tuberculosis*). To obtain TDM and TMM, cell pellets were extracted with chloroform:methanol (2:1). The extracted lipids were separated by TLC (HPTLC silica gel, Millipore, Billerica, MA) with chloroform:methanol:acetone (90:15:10) and chloroform:methenol:H_2O (80:20:2) for TDM and TMM, respectively (35, 90). 5% H_2SO_4 in ethanol was used to develop TLC. Covalent mycolate extraction was adopted from (91). Briefly, mycolic-arabinogalactan-peptidoglycan (mAGP) complex was extracted from 100 mL of culture as described (91). The pellet was resuspended in PBS and sonicated to lyse the cells. Lysates were centrifuged and pellets were collected and washed with PBS. The pellets were resupended in 2% SDS in PBS and incubated at 80°C for 3 hours with intermediate shaking. They were then resuspended in 1% SDS, centrifuged, and washed twice with water, once with 80% acetone, and once with 100% acetone. Pellet were dried to obtain the final mAGP complex. Samples were normalized by mAGP weight, then resuspended in PBS + 0.05% Tween-80 (PBST) by water bath sonication. To extract mycolic acids from mAGP, the suspension was treated with 5% tetrabutylammonium hydroxide (TBAH) overnight with shaking. The extracted mycolic acids were seprated by treating with equal volume of dichloromethane followed by treatment with equal volume of 0.25 M HCl and water-washed as described (91). To

extract free mycolic acids from culture supernatants, the OD_{600} of *M. smegmatis* grown for 24 hours in 7H9T-2% or 0.02% glucose were normalized to 1 with 7H9T. The normalized cultures were centrifuged at 10000xg for 5 minutes and superntants were collected and passed through a 0.25 µm syringe filter. Supernatants (1 mL) were treated with 5% TBAH for 1 hour followed by an equal amount of dichloromethane and overnight incubation at room temperature with shaking. The suspension was then centrifuged at 10000xg and the lower organic layer was removed. The organic layer was evaporated and the pellet was mixed with 40 µL chloroform:methenol (2:1). Mycolic acids were separated by TLC using chloroform:methanol (96:4) as described (7). 5% molybdophosphoric acid in ethanol was was used to develop the TLC.

Fluorescent glucose labeling. *M. smegmatis* cultured in 0.02% glucose-supplemented 7H9T was normalized to OD_{600} of 1.0 in fresh medium and treated with 5 µM of the fluorescent glucose analogue 2-(N-(7-Nitrobenz-2-oxa-1,3-diazol-4-yl)Amino)-2-Deoxyglucose (2-NBDG; abcam, Cambridge, MA) for 2 hours at 37°C with shaking. Cultures were then centrifuged at RT for 5 minutes, 4000 rpm and washed twice with PBST. After normalizing to wet weight, pellets were extracted with chloroform:methanol (2:1) overnight. The organic extracts were separated from the cell suspension by centrifugation at RT for 15 minutes, 12,000 rpm then treated with one volume of H_2O for 15 min at RT. The aqueous and organic layers were separated from each other suspension by centrifugation at RT for 5 minutes, 12,000 rpm then run on TLC using chloroform:methanol: H_2O (80:20:2) and 1-propanol:ethylacetate:water (6:1:3),

respectively. The fluorescence of TLC was recorded by ImageQuant system (GE Healthcare) or developed using 5% H_2SO_4 in ethanol.

Propidium iodide (PI). We assessed PI uptake as described (92). Briefly, 50 µg/mL PI was added to *M. smegmatis* that had been cultured in 0.02% or 2% glucose. After incubating for 15 minutes at 37°C, samples were washed once with PBS and fluorescence was measured by flow cytometry.

Cell envelope labeling. Probes used in this study include alkDala (50 µM), HADA (500 µM), O-AlkTMM (50 µM), N-AlkTMM (250 µM) and 6-TreAz (50 µM). *M. smegmatis* labeling was performed mainly as described (38). Briefly, the OD_{600} was normalized to 1 in the same medium. Cultures were shaken in the presence of probes for 30 min at 37°C for *M. smegmatis*. After incubation the cultures were washed twice with PBST and fixed or not with 2% formaldehyde at room temperature for 10 minutes. After fixation, cultures were washed with PBST. Alkynes were detected by CuAAC reaction with carboxyrhodamine 110 azide (Click Chemistry Tools, Scottsdale, AZ). Azides were detected on live, unfixed cells by SPAAC reaction with DBCO-Cy5 (Click Chemistry Tools, Scottsdale, AZ). Finally, cultures were washed thrice with PBST and fluorescence was measured by flow cytometery. For *M. tuberculosis,* the OD_{600} for carbon-starved and unstarved cultures were normalized to 1 in the same media. Cultures were shaken in the presence of probes for 3 hours at 37°C then washed twice with PBST and subjected to

SPAAC overnight at 37°C. Cultures were washed thrice with PBST and fixed with 4% formaldehyde overnight at room temperature prior to removal from the BSL3 facility.

Microscopy analysis. Fluorescence microscopy and image quantitation was performed exactly as described in (38).

qRT-PCR. *M. smegmatis* was cultured in 0.02% glucose medium for 24 hours. Cell pellets were resuspended in 1 mL of TRIzol reagent (Invitrogen, Carlsbad, CA) prior to bead-beating (MP Biochemicals Lysing Matrix B). After bead-beating, 300 µL chloroform was added to each tube. The tubes were centrifuged at 14000 rpm for 15 min at 4°C. The upper aqueous layer was removed and resuspended in 600 µL isopropanol in a fresh tube. The tube was kept at -20°C for 1 hour to overnight and then centrifuged for 20 minute at 4°C, 14000 rpm to precipitate the RNA. The RNA-containing pellet was washed once with 75% ethanol by centrifugation for 5 minute at 4°C, 14000rpm and resuspended in RNase-free H_2O. 20 µg of RNA was treated with 2.5 µL DNase (TURBO™ DNase, Ambion, Carlsbad, CA) in a final volume of 100 µL. The reaction was incubated for 2 hours at 37°C. The RNA was then cleaned up following the manufacturer's instructions for the Qiagen RNeasy Mini Kit (Qiagen). cDNA synthesis was carried out using 5 µg of the cleaned-up RNA following the manufacturer's instructions for SuperScript IV Reverse Transcriptase (Invitrogen). The cDNA was then used for qRT-PCR reactions (iTaq Universal SYBR Green Supermix, BioRad, Hercules, CA). We used the *sigA* gene as our internal control. Primers are listed in **Table 2.**

Table 1: Strains used in this study.

Strain Name	Source
Immortalized C57BL/6 BMDM	Dr. Christopher Sassetti (93)
M. smegmatis mc^{2}155	NC_008596 in GenBank (94)
M. smegmatis Δ*sugC*	Dr. Rainer Kalscheuer (20)
M. smegmatis Δ*sugC* pMV361-*sugC*	Dr. Ben Swarts (95, 96)
M. smegmatis Δ*otsA*	Dr. Rainer Kalscheuer (51)
M. smegmatis Δ*treYZ*	Dr. Rainer Kalscheuer (51)
M. smegmatis Δ*treS*	Dr. Rainer Kalscheuer (51)
M. smegmatis Δ*tre*	Dr. Rainer Kalscheuer (48)
M. smegmatis Δ*otsA* pYAB-*tre*	This study
M. smegmatis Δ*treYZ* pYAB-*tre*	This study
M. smegmatis pYAB	Dr. Yasu Morita (97, 98)
M. smegmatis pYAB-*tre*	This study
M. tuberculosis H37Rv	Dr. Rainer Kalscheuer (20)
M. tuberculosis Δ*sugC*	Dr. Rainer Kalscheuer (20)
M. tuberculosis Δ*lpqY*	Dr. Rainer Kalscheuer (20)
M. tuberculosis Δ*sugC* pMV306-*sugC*	Dr. Rainer Kalscheuer (20, 95)
E. coli XL-1 blue	Agilent technologies

Table 2: Primer names and sequences.

Primer name	Sequence
4535For_Acet	Tgatgtgctctagagttctgcaacagaccgagcc
4535Rev_Acet	Ggcctgatctagacatcggggcgttcgcgg
RT-otsA-For	Actacaccaagggcatcgac
RT-otsA-Rev	Tcgcgatgtagctctcgac
RT-otsB-For (MSMEG_3954)	Aacgagagcctggtcaatct
RT-otsB-Rev (MSMEG_3954)	Agggtctgctggtaggactg
RT-otsB-For (MSMEG_6043)	Gtgagtctttcgggggatct
RT-otsB-Rev (MSMEG_6043)	Aatcggatgtgaccagcag
RT-treY-For	Ctctcgacgtatcggttgc
RT-treY-Rev	Aggatgggggacagatacac
RT-treZ-For	Ctcgactacctggtcgatctc
RT-treZ-Rev	Acctccgtagggttcgtgta
ForsigA	Gggctacaagttctcgacct
RevsigA	Ccgagcttgttgatcacctc

Acknowledgments

We are grateful to Drs. Rainier Kalscheuer for *M. smegmatis* and *M. tuberculosis* strains, Christopher Sassetti for immortalized bone marrow-derived macrophages, Yasu Morita for assistance with thin layer chromatography and Hyungjin Eoh for thoughtful feedback on the manuscript. Research was supported by NIH DP2 AI138238 (M.S.S.) and NSF CAREER 1654408 (B.M.S.).

Author Contributions

A.A.P. Conceptualization, methodology, validation, formal analysis, investigation, visualization, project administration, data curation, writing – reviewing and editing. C.R.C. Validation, investigation, writing – reviewing and editing, data curation, software. J.G. Supervision, writing – reviewing and editing. B.M.S. writing – Methodology, writing – reviewing and editing, resources, funding acquisition. M.S.S. Conceptualization, methodology, visualization, resources, writing – Original Draft, reviewing and editing, supervision, project administration, funding acquisition.

References

1. Puffal J, Garcia-Heredia A, Rahlwes KC, Siegrist MS, Morita YS. 2018. Spatial control of cell envelope biosynthesis in mycobacteria. Pathog Dis 76.
2. Lee WB, Kang JS, Choi WY, Zhang Q, Kim CH, Choi UY, Kim-Ha J, Kim YJ. 2016. Mincle-mediated translational regulation is required for strong nitric oxide production and inflammation resolution. Nat Commun 7:11322.
3. Yang Y, Kulka K, Montelaro RC, Reinhart TA, Sissons J, Aderem A, Ojha AK. 2014. A hydrolase of trehalose dimycolate induces nutrient influx and stress sensitivity to balance intracellular growth of *Mycobacterium tuberculosis*. Cell Host Microbe 15:153-63.
4. Gebhardt H, Meniche X, Tropis M, Kramer R, Daffe M, Morbach S. 2007. The key role of the mycolic acid content in the functionality of the cell wall permeability barrier in Corynebacterineae. Microbiology 153:1424-34.
5. Galagan JE, Minch K, Peterson M, Lyubetskaya A, Azizi E, Sweet L, Gomes A, Rustad T, Dolganov G, Glotova I, Abeel T, Mahwinney C, Kennedy AD, Allard R, Brabant W, Krueger A, Jaini S, Honda B, Yu WH, Hickey MJ, Zucker J, Garay C, Weiner B, Sisk P, Stolte C, Winkler JK, Van de Peer Y, Iazzetti P, Camacho D, Dreyfuss J, Liu Y, Dorhoi A, Mollenkopf HJ, Drogaris P, Lamontagne J, Zhou Y, Piquenot J, Park ST, Raman S, Kaufmann SH, Mohney RP, Chelsky D, Moody DB, Sherman DR, Schoolnik GK. 2013. The *Mycobacterium tuberculosis* regulatory network and hypoxia. Nature 499:178-83.
6. Eoh H, Wang Z, Layre E, Rath P, Morris R, Branch Moody D, Rhee KY. 2017. Metabolic anticipation in *Mycobacterium tuberculosis*. Nat Microbiol 2:17084.
7. Ojha AK, Trivelli X, Guerardel Y, Kremer L, Hatfull GF. 2010. Enzymatic hydrolysis of trehalose dimycolate releases free mycolic acids during mycobacterial growth in biofilms. J Biol Chem 285:17380-9.
8. Kieser KJ, Rubin EJ. 2014. How sisters grow apart: mycobacterial growth and division. Nat Rev Microbiol 12:550-62.

9. Baker JJ, Abramovitch RB. 2018. Genetic and metabolic regulation of *Mycobacterium tuberculosis* acid growth arrest. Sci Rep 8:4168.
10. Bacon J, Alderwick LJ, Allnutt JA, Gabasova E, Watson R, Hatch KA, Clark SO, Jeeves RE, Marriott A, Rayner E, Tolley H, Pearson G, Hall G, Besra GS, Wernisch L, Williams A, Marsh PD. 2014. Non-replicating *Mycobacterium tuberculosis* elicits a reduced infectivity profile with corresponding modifications to the cell wall and extracellular matrix. PLoS ONE 9:e87329.
11. Shui G, Bendt AK, Pethe K, Dick T, Wenk MR. 2007. Sensitive profiling of chemically diverse bioactive lipids. J Lipid Res 48:1976-84.
12. Bhamidi S, Scherman MS, Jones V, Crick DC, Belisle JT, Brennan PJ, McNeil MR. 2011. Detailed structural and quantitative analysis reveals the spatial organization of the cell walls of in vivo grown Mycobacterium leprae and in vitro grown *Mycobacterium tuberculosis*. J Biol Chem 286:23168-77.
13. Dulberger CL, Rubin EJ, Boutte CC. 2020. The mycobacterial cell envelope - a moving target. Nat Rev Microbiol 18:47-59.
14. Quemard A. 2016. New Insights into the Mycolate-Containing Compound Biosynthesis and Transport in Mycobacteria. Trends Microbiol 24:725-738.
15. Holmes NJ, Kavunja HW, Yang Y, Vannest BD, Ramsey CN, Gepford DM, Banahene N, Poston AW, Piligian BF, Ronning DR, Ojha AK, Swarts BM. 2019. A FRET-Based Fluorogenic Trehalose Dimycolate Analogue for Probing Mycomembrane-Remodeling Enzymes of Mycobacteria. ACS Omega 4:4348-4359.
16. Dunphy KY, Senaratne RH, Masuzawa M, Kendall LV, Riley LW. 2010. Attenuation of *Mycobacterium tuberculosis* functionally disrupted in a fatty acyl-coenzyme A synthetase gene *fadD5*. J Infect Dis 201:1232-9.
17. Wilburn KM, Fieweger RA, VanderVen BC. 2018. Cholesterol and fatty acids grease the wheels of *Mycobacterium tuberculosis* pathogenesis. Pathog Dis 76.
18. Cantrell SA, Leavell MD, Marjanovic O, Iavarone AT, Leary JA, Riley LW. 2013. Free mycolic acid accumulation in the cell wall of the *mce1* operon mutant strain of *Mycobacterium tuberculosis*. J Microbiol 51:619-26.
19. Forrellad MA, McNeil M, Santangelo Mde L, Blanco FC, Garcia E, Klepp LI, Huff J, Niederweis M, Jackson M, Bigi F. 2014. Role of the Mce1 transporter in the lipid homeostasis of *Mycobacterium tuberculosis*. Tuberculosis (Edinb) 94:170-7.
20. Kalscheuer R, Weinrick B, Veeraraghavan U, Besra GS, Jacobs WR, Jr. 2010. Trehalose-recycling ABC transporter LpqY-SugA-SugB-SugC is essential for virulence of *Mycobacterium tuberculosis*. Proc Natl Acad Sci U S A 107:21761-6.
21. Nobre A, Alarico S, Maranha A, Mendes V, Empadinhas N. 2014. The molecular biology of mycobacterial trehalose in the quest for advanced tuberculosis therapies. Microbiology 160:1547-70.
22. Shleeva MO, Trutneva KA, Demina GR, Zinin AI, Sorokoumova GM, Laptinskaya PK, Shumkova ES, Kaprelyants AS. 2017. Free Trehalose Accumulation in Dormant *Mycobacterium smegmatis* Cells and Its Breakdown in Early Resuscitation Phase. Front Microbiol 8:524.
23. Lee JJ, Lee SK, Song N, Nathan TO, Swarts BM, Eum SY, Ehrt S, Cho SN, Eoh H. 2019. Transient drug-tolerance and permanent drug-resistance rely on the trehalose-catalytic shift in *Mycobacterium tuberculosis*. Nat Commun 10:2928.

24. Brynildsen MP, Winkler JA, Spina CS, MacDonald IC, Collins JJ. 2013. Potentiating antibacterial activity by predictably enhancing endogenous microbial ROS production. Nat Biotechnol 31:160-5.
25. Adolfsen KJ, Brynildsen MP. 2015. Futile cycling increases sensitivity toward oxidative stress in *Escherichia coli.* Metab Eng 29:26-35.
26. Koebmann BJ, Westerhoff HV, Snoep JL, Nilsson D, Jensen PR. 2002. The glycolytic flux in *Escherichia coli* is controlled by the demand for ATP. J Bacteriol 184:3909-16.
27. Mok WW, Park JO, Rabinowitz JD, Brynildsen MP. 2015. RNA Futile Cycling in Model Persisters Derived from MazF Accumulation. mBio 6:e01588-15.
28. Izallalen M, Mahadevan R, Burgard A, Postier B, Didonato R, Jr., Sun J, Schilling CH, Lovley DR. 2008. *Geobacter sulfurreducens* strain engineered for increased rates of respiration. Metab Eng 10:267-75.
29. Yang JH, Bening SC, Collins JJ. 2017. Antibiotic efficacy-context matters. Curr Opin Microbiol 39:73-80.
30. Vilcheze C, Hartman T, Weinrick B, Jain P, Weisbrod TR, Leung LW, Freundlich JS, Jacobs WR, Jr. 2017. Enhanced respiration prevents drug tolerance and drug resistance in *Mycobacterium tuberculosis*. Proc Natl Acad Sci U S A 114:4495-4500.
31. Danelishvili L, Shulzhenko N, Chinison JJJ, Babrak L, Hu J, Morgun A, Burrows G, Bermudez LE. 2017. *Mycobacterium tuberculosis* Proteome Response to Antituberculosis Compounds Reveals Metabolic "Escape" Pathways That Prolong Bacterial Survival. Antimicrob Agents Chemother 61.
32. Rengarajan J, Bloom BR, Rubin EJ. 2005. Genome-wide requirements for *Mycobacterium tuberculosis* adaptation and survival in macrophages. Proc Natl Acad Sci U S A 102:8327-32.
33. Sassetti CM, Rubin EJ. 2003. Genetic requirements for mycobacterial survival during infection. Proc Natl Acad Sci U S A 100:12989-94.
34. Yang Y, Bhatti A, Ke D, Gonzalez-Juarrero M, Lenaerts A, Kremer L, Guerardel Y, Zhang P, Ojha AK. 2013. Exposure to a cutinase-like serine esterase triggers rapid lysis of multiple mycobacterial species. J Biol Chem 288:382-92.
35. Foley HN, Stewart JA, Kavunja HW, Rundell SR, Swarts BM. 2016. Bioorthogonal Chemical Reporters for Selective In Situ Probing of Mycomembrane Components in Mycobacteria. Angew Chem Int Ed Engl 55:2053-7.
36. Matsunaga I, Naka T, Talekar RS, McConnell MJ, Katoh K, Nakao H, Otsuka A, Behar SM, Yano I, Moody DB, Sugita M. 2008. Mycolyltransferase-mediated glycolipid exchange in Mycobacteria. J Biol Chem 283:28835-41.
37. Gavalda S, Bardou F, Laval F, Bon C, Malaga W, Chalut C, Guilhot C, Mourey L, Daffe M, Quemard A. 2014. The polyketide synthase Pks13 catalyzes a novel mechanism of lipid transfer in mycobacteria. Chem Biol 21:1660-9.
38. Garcia-Heredia A, Pohane AA, Melzer ES, Carr CR, Fiolek TJ, Rundell SR, Chuin Lim H, Wagner JC, Morita YS, Swarts BM, Siegrist MS. 2018. Peptidoglycan precursor synthesis along the sidewall of pole-growing mycobacteria. eLife 7.
39. Jackson M, Raynaud C, Laneelle MA, Guilhot C, Laurent-Winter C, Ensergueix D, Gicquel B, Daffe M. 1999. Inactivation of the antigen 85C gene profoundly affects

the mycolate content and alters the permeability of the *Mycobacterium tuberculosis* cell envelope. Mol Microbiol 31:1573-87.
40. Meniche X, Otten R, Siegrist MS, Baer CE, Murphy KC, Bertozzi CR, Sassetti CM. 2014. Subpolar addition of new cell wall is directed by DivIVA in mycobacteria. Proc Natl Acad Sci U S A doi:10.1073/pnas.1402158111.
41. Boutte CC, Baer CE, Papavinasasundaram K, Liu W, Chase MR, Meniche X, Fortune SM, Sassetti CM, Ioerger TR, Rubin EJ. 2016. A cytoplasmic peptidoglycan amidase homologue controls mycobacterial cell wall synthesis. eLife 5.
42. Siegrist MS, Whiteside S, Jewett JC, Aditham A, Cava F, Bertozzi CR. 2013. (D)-amino acid chemical reporters reveal peptidoglycan dynamics of an intracellular pathogen. ACS Chem Biol 8:500-5.
43. Botella H, Yang G, Ouerfelli O, Ehrt S, Nathan CF, Vaubourgeix J. 2017. Distinct Spatiotemporal Dynamics of Peptidoglycan Synthesis between *Mycobacterium smegmatis* and *Mycobacterium tuberculosis*. MBio 8.
44. Schubert K, Sieger B, Meyer F, Giacomelli G, Bohm K, Rieblinger A, Lindenthal L, Sachs N, Wanner G, Bramkamp M. 2017. The Antituberculosis Drug Ethambutol Selectively Blocks Apical Growth in CMN Group Bacteria. MBio 8.
45. Rodriguez-Rivera FP, Zhou X, Theriot JA, Bertozzi CR. 2017. Visualization of mycobacterial membrane dynamics in live cells. J Am Chem Soc 139:3488-3495.
46. Rodriguez-Rivera FP, Zhou X, Theriot JA, Bertozzi CR. 2018. Acute modulation of mycobacterial cell envelope biogenesis by front-line TB drugs. Angew Chem Int Ed Engl doi:10.1002/anie.201712020.
47. Baranowski C, Welsh MA, Sham LT, Eskandarian HA, Lim HC, Kieser KJ, Wagner JC, McKinney JD, Fantner GE, Ioerger TR, Walker S, Bernhardt TG, Rubin EJ, Rego EH. 2018. Maturing *Mycobacterium smegmatis* peptidoglycan requires non-canonical crosslinks to maintain shape. Elife 7.
48. Kamariza M, Shieh P, Ealand CS, Peters JS, Chu B, Rodriguez-Rivera FP, Babu Sait MR, Treuren WV, Martinson N, Kalscheuer R, Kana BD, Bertozzi CR. 2018. Rapid detection of *Mycobacterium tuberculosis* in sputum with a solvatochromic trehalose probe. Sci Transl Med 10.
49. Garcia-Heredia A, Pohane AA, Melzer ES, Carr CR, Fiolek TJ, Rundell SR, Lim HC, Wagner JC, Morita YS, Swarts BM, Siegrist MS. 2018. Peptidoglycan precursor synthesis along the sidewall of pole-growing mycobacteria. eLife 7.
50. Kalscheuer R, Koliwer-Brandl H. 2014. Genetics of Mycobacterial Trehalose Metabolism. Microbiol Spectr 2.
51. Miah F, Koliwer-Brandl H, Rejzek M, Field RA, Kalscheuer R, Bornemann S. 2013. Flux through trehalose synthase flows from trehalose to the alpha anomer of maltose in mycobacteria. Chem Biol 20:487-93.
52. Kalscheuer R, Syson K, Veeraraghavan U, Weinrick B, Biermann KE, Liu Z, Sacchettini JC, Besra G, Bornemann S, Jacobs WR, Jr. 2010. Self-poisoning of *Mycobacterium tuberculosis* by targeting GlgE in an alpha-glucan pathway. Nat Chem Biol 6:376-84.
53. Swarts BM, Holsclaw CM, Jewett JC, Alber M, Fox DM, Siegrist MS, Leary JA, Kalscheuer R, Bertozzi CR. 2012. Probing the mycobacterial trehalome with bioorthogonal chemistry. J Am Chem Soc 134:16123-6.

54. Yang NJ, Hinner MJ. 2015. Getting across the cell membrane: an overview for small molecules, peptides, and proteins. Methods Mol Biol 1266:29-53.
55. Vilcheze C, Hartman T, Weinrick B, Jacobs WR, Jr. 2013. *Mycobacterium tuberculosis* is extraordinarily sensitive to killing by a vitamin C-induced Fenton reaction. Nat Commun 4:1881.
56. Owusu-Ansah E, Yavari A, Banerjee U. 2008. A protocol for *in vivo* detection of reactive oxygen species.
57. Newton GL, Buchmeier N, Fahey RC. 2008. Biosynthesis and functions of mycothiol, the unique protective thiol of Actinobacteria. Microbiol Mol Biol Rev 72:471-94.
58. Kumar A, Farhana A, Guidry L, Saini V, Hondalus M, Steyn AJ. 2011. Redox homeostasis in mycobacteria: the key to tuberculosis control? Expert Rev Mol Med 13:e39.
59. Wayne LG, Hayes LG. 1996. An in vitro model for sequential study of shiftdown of *Mycobacterium tuberculosis* through two stages of nonreplicating persistence. Infect Immun 64:2062-9.
60. Wang C, Pi L, Jiang S, Yang M, Shu C, Zhou E. 2018. ROS and trehalose regulate sclerotial development in *Rhizoctonia solani* AG-1 IA. Fungal Biol 122:322-332.
61. Lunn JE, Delorge I, Figueroa CM, Van Dijck P, Stitt M. 2014. Trehalose metabolism in plants. Plant J 79:544-67.
62. Kuczynska-Wisnik D, Stojowska K, Matuszewska E, Leszczynska D, Algara MM, Augustynowicz M, Laskowska E. 2015. Lack of intracellular trehalose affects formation of *Escherichia coli* persister cells. Microbiology 161:786-96.
63. Luo Y, Li W-M, Wang W. 2008. Trehalose: Protector of antioxidant enzymes or reactive oxygen species scavenger under heat stress. Environmental and Experimental Botany 2008 v.63 no.1-3:pp. 378-384.
64. Korte J, Alber M, Trujillo CM, Syson K, Koliwer-Brandl H, Deenen R, Kohrer K, DeJesus MA, Hartman T, Jacobs WR, Jr., Bornemann S, Ioerger TR, Ehrt S, Kalscheuer R. 2016. Trehalose-6-Phosphate-Mediated Toxicity Determines Essentiality of OtsB2 in *Mycobacterium tuberculosis In Vitro* and in Mice. PLoS Pathog 12:e1006043.
65. Hu K, Li Y, Rotenberg SA, Amatore C, Mirkin MV. 2019. Electrochemical Measurements of Reactive Oxygen and Nitrogen Species inside Single Phagolysosomes of Living Macrophages. J Am Chem Soc 141:4564-4568.
66. Nathan CF, Murray HW, Wiebe ME, Rubin BY. 1983. Identification of interferon-gamma as the lymphokine that activates human macrophage oxidative metabolism and antimicrobial activity. J Exp Med 158:670-89.
67. Ehrt S, Schnappinger D. 2009. Mycobacterial survival strategies in the phagosome: defence against host stresses. Cell Microbiol 11:1170-8.
68. Stallings CL, Glickman MS. 2010. Is *Mycobacterium tuberculosis* stressed out? A critical assessment of the genetic evidence. Microbes Infect 12:1091-101.
69. Andries K, Verhasselt P, Guillemont J, Gohlmann HW, Neefs JM, Winkler H, Van Gestel J, Timmerman P, Zhu M, Lee E, Williams P, de Chaffoy D, Huitric E, Hoffner S, Cambau E, Truffot-Pernot C, Lounis N, Jarlier V. 2005. A diarylquinoline drug active on the ATP synthase of *Mycobacterium tuberculosis*. Science 307:223-7.

70. Koul A, Dendouga N, Vergauwen K, Molenberghs B, Vranckx L, Willebrords R, Ristic Z, Lill H, Dorange I, Guillemont J, Bald D, Andries K. 2007. Diarylquinolines target subunit c of mycobacterial ATP synthase. Nat Chem Biol 3:323-4.
71. Koul A, Vranckx L, Dhar N, Gohlmann HW, Ozdemir E, Neefs JM, Schulz M, Lu P, Mortz E, McKinney JD, Andries K, Bald D. 2014. Delayed bactericidal response of *Mycobacterium tuberculosis* to bedaquiline involves remodelling of bacterial metabolism. Nat Commun 5:3369.
72. Lamprecht DA, Finin PM, Rahman MA, Cumming BM, Russell SL, Jonnala SR, Adamson JH, Steyn AJ. 2016. Turning the respiratory flexibility of *Mycobacterium tuberculosis* against itself. Nat Commun 7:12393.
73. Lee BS, Kalia NP, Jin XEF, Hasenoehrl EJ, Berney M, Pethe K. 2019. Inhibitors of energy metabolism interfere with antibiotic-induced death in mycobacteria. J Biol Chem 294:1936-1943.
74. Shetty A, Dick T. 2018. Mycobacterial Cell Wall Synthesis Inhibitors Cause Lethal ATP Burst. Front Microbiol 9:1898.
75. Seiler P, Ulrichs T, Bandermann S, Pradl L, Jorg S, Krenn V, Morawietz L, Kaufmann SH, Aichele P. 2003. Cell-wall alterations as an attribute of *Mycobacterium tuberculosis* in latent infection. J Infect Dis 188:1326-31.
76. Vilcheze C, Kremer L. 2017. Acid-Fast Positive and Acid-Fast Negative *Mycobacterium tuberculosis*: The Koch Paradox. Microbiol Spectr 5.
77. Cadena AM, Fortune SM, Flynn JL. 2017. Heterogeneity in tuberculosis. Nat Rev Immunol 17:691-702.
78. Siegrist MS, Swarts BM, Fox DM, Lim SA, Bertozzi CR. 2015. Illumination of growth, division and secretion by metabolic labeling of the bacterial cell surface. FEMS Microbiol Rev 39:184-202.
79. Karakousis PC, Bishai WR, Dorman SE. 2004. *Mycobacterium tuberculosis* cell envelope lipids and the host immune response. Cell Microbiol 6:105-16.
80. Rajni, Rao N, Meena LS. 2011. Biosynthesis and Virulent Behavior of Lipids Produced by *Mycobacterium tuberculosis*: LAM and Cord Factor: An Overview. Biotechnol Res Int 2011:274693.
81. Rafidinarivo E, Laneelle MA, Montrozier H, Valero-Guillen P, Astola J, Luquin M, Prome JC, Daffe M. 2009. Trafficking pathways of mycolic acids: structures, origin, mechanism of formation, and storage form of mycobacteric acids. J Lipid Res 50:477-90.
82. Puech V, Guilhot C, Perez E, Tropis M, Armitige LY, Gicquel B, Daffe M. 2002. Evidence for a partial redundancy of the fibronectin-binding proteins for the transfer of mycoloyl residues onto the cell wall arabinogalactan termini of *Mycobacterium tuberculosis*. Mol Microbiol 44:1109-22.
83. Jamet S, Quentin Y, Coudray C, Texier P, Laval F, Daffe M, Fichant G, Cam K. 2015. Evolution of Mycolic Acid Biosynthesis Genes and Their Regulation during Starvation in *Mycobacterium tuberculosis*. J Bacteriol 197:3797-811.
84. Betts JC, Lukey PT, Robb LC, McAdam RA, Duncan K. 2002. Evaluation of a nutrient starvation model of *Mycobacterium tuberculosis* persistence by gene and protein expression profiling. Mol Microbiol 43:717-31.
85. Zhao DQ, Li TT, Hao ZJ, Cheng ML, Tao J. 2019. Exogenous trehalose confers high temperature stress tolerance to herbaceous peony by enhancing antioxidant

systems, activating photosynthesis, and protecting cell structure. Cell Stress Chaperones 24:247-257.
86. Elbein AD, Pan YT, Pastuszak I, Carroll D. 2003. New insights on trehalose: a multifunctional molecule. Glycobiology 13:17R-27R.
87. Dwyer DJ, Belenky PA, Yang JH, MacDonald IC, Martell JD, Takahashi N, Chan CT, Lobritz MA, Braff D, Schwarz EG, Ye JD, Pati M, Vercruysse M, Ralifo PS, Allison KR, Khalil AS, Ting AY, Walker GC, Collins JJ. 2014. Antibiotics induce redox-related physiological alterations as part of their lethality. Proc Natl Acad Sci U S A 111:E2100-9.
88. Lobritz MA, Belenky P, Porter CB, Gutierrez A, Yang JH, Schwarz EG, Dwyer DJ, Khalil AS, Collins JJ. 2015. Antibiotic efficacy is linked to bacterial cellular respiration. Proc Natl Acad Sci U S A 112:8173-80.
89. Bliss CI. 1956. The calculation of microbial assays. Bacteriol Rev 20:243-58.
90. Touchette MH, Van Vlack ER, Bai L, Kim J, Cognetta AB, 3rd, Previti ML, Backus KM, Martin DW, Cravatt BF, Seeliger JC. 2017. A Screen for Protein-Protein Interactions in Live Mycobacteria Reveals a Functional Link between the Virulence-Associated Lipid Transporter LprG and the Mycolyltransferase Antigen 85A. ACS Infect Dis 3:336-348.
91. Payne K, Sun Q, Sacchettini J, Hatfull GF. 2009. Mycobacteriophage Lysin B is a novel mycolylarabinogalactan esterase. Mol Microbiol 73:367-81.
92. Sharma A, Pohane AA, Bansal S, Bajaj A, Jain V, Srivastava A. 2015. Cell penetrating synthetic antimicrobial peptides (SAMPs) exhibiting potent and selective killing of mycobacterium by targeting its DNA. Chemistry 21:3540-5.
93. Nambi S, Long JE, Mishra BB, Baker R, Murphy KC, Olive AJ, Nguyen HP, Shaffer SA, Sassetti CM. 2015. The Oxidative Stress Network of *Mycobacterium tuberculosis* Reveals Coordination between Radical Detoxification Systems. Cell Host Microbe 17:829-37.
94. Snapper SB, Melton RE, Mustafa S, Kieser T, Jacobs WR, Jr. 1990. Isolation and characterization of efficient plasmid transformation mutants of *Mycobacterium smegmatis*. Mol Microbiol 4:1911-9.
95. Stover CK, de la Cruz VF, Fuerst TR, Burlein JE, Benson LA, Bennett LT, Bansal GP, Young JF, Lee MH, Hatfull GF, et al. 1991. New use of BCG for recombinant vaccines. Nature 351:456-60.
96. Urbanek BL, Wing DC, Haislop KS, Hamel CJ, Kalscheuer R, Woodruff PJ, Swarts BM. 2014. Chemoenzymatic synthesis of trehalose analogues: rapid access to chemical probes for investigating mycobacteria. Chembiochem 15:2066-70.
97. Hayashi JM, Luo CY, Mayfield JA, Hsu T, Fukuda T, Walfield AL, Giffen SR, Leszyk JD, Baer CE, Bennion OT, Madduri A, Shaffer SA, Aldridge BB, Sassetti CM, Sandler SJ, Kinoshita T, Moody DB, Morita YS. 2016. Spatially distinct and metabolically active membrane domain in mycobacteria. Proc Natl Acad Sci U S A 113:5400-5.
98. Rahlwes KC, Ha SA, Motooka D, Mayfield JA, Baumoel LR, Strickland JN, Torres-Ocampo AP, Nakamura S, Morita YS. 2017. The cell envelope-associated phospholipid-binding protein LmeA is required for mannan polymerization in mycobacteria. J Biol Chem 292:17407-17417.

99. Schneider CA, Rasband WS, Eliceiri KW. 2012. NIH Image to ImageJ: 25 years of image analysis. Nat Methods 9:671-5.

Figure Legends

Figure 1. Mycomembrane synthesis and degradation are active under carbon limitation.

(A) Mycomembrane synthesis and degradation. TMM, trehalose monomycolate; TDM, trehalose dimycolate; AG, arabinogalactan; AGM, arabinogalactan mycolates; MA, free mycolic acids; TDMH, TDM hydrolase.

(B) TDM turnover under nutrient deprivation. *M. smegmatis* was cultured in 0.02% glucose-supplemented medium in the presence of metabolic probes O-AlkTMM (primarily labels AGM), N-AlkTMM (labels TDM) or HADA (labels cell wall peptidoglycan). After 24 hours, cultures were washed and resuspended in probe-free medium. Aliquots were removed 0, 4 and 8 hours into the chase and fixed with 2% formaldehyde. Alkynes were detected by copper-catalyzed azide-alkyne cycloaddition (CuAAC) reaction with carboxyrhodamine 110 azide. Fluorescence was quantitated by flow cytometry, with the median fluorescence intensities normalized to the initial, 0 h time point for each probe. Experiment was performed three times in triplicate; one representative experiment shown.

(C) Metabolic labeling of *M. smegmatis* in 0.02% glucose-supplemented medium with O-AlkTMM, N-AlkTMM and alkDala (labels peptidoglycan). Alkynes were detected by

CuAAC reaction with carboxyrhodamine 110 azide. Data were normalized to labeling in 2% glucose-supplemented medium and plotted from four independent experiments.

(D) Quantitation of thin-layer chromatography (TLC) of different mycomembrane components for *M. smegmatis* in 0.02%-supplemented medium. TDM, trehalose dimycolate; CS-MA, free, culture supernatant mycolic acids; AGM-MA, mycolic acids released from arabinogalactan. TLCs were scanned and processed in ImageJ (99). Data are normalized to TLCs from samples taken from *M. smegmatis* cultured in 2% glucose-supplemented medium and plotted from three independent experiments. Representative TLCs, **Figure S2**.

(E) Propidium iodide (PI) staining of *M. smegmatis* during adaptation to low carbon. *M. smegmatis* was cultured in 0.02% glucose-supplemented medium. Aliquots were removed 13, 24 and 48 hours and incubated with PI. Fluorescence was quantitated by flow cytometry and median fluorescence intensity (MFI) was plotted. Experiment was performed three times in triplicate; one representative experiment shown.

(F) O-AlkTMM labeling of *M. smegmatis* AGM in 2% or 0.02% glucose-supplemented medium. Alkynes were detected by CuAAC reaction with carboxyrhodamine 110 azide. Left, fluorescence microscopy. Scale bars, 5 μM. Right, cellular fluorescence was quantitated for cells lacking visible septa from three independent experiments. Signal was normalized to both cell length and to total fluorescence intensity. Cells were oriented such that the brighter pole is on the right hand side of the graph. A.U., arbitrary units.

(G) Quantification of trehalose from supernatants of wild-type and Δ*sugC M. smegmatis* cultured in 2% or 0.02% glycerol supplemented medium. Experiment was performed at least three times in triplicate; one representative experiment shown.

Error bars, standard deviation. Statistical significance of 0.02% vs. 2% glucose or glycerol samples from three independent experiments was assessed by two-tailed Student's t test. *, $p<0.05$; **, $p<0.005$.

Figure 2. Trehalose cycling supports mycomembrane metabolism during carbon limitation.

(A) Potential fates of recycled trehalose in catabolism (trehalase [Tre] or TreS) or in trehalose monomycoate (TMM) biosynthesis.

(B) and (C), Survival of wild-type, Δ*sugC,* complemented Δ*sugC* (CΔ*sugC*), Δ*treS* and Δ*tre M. smegmatis* in 0.02% glucose-supplemented medium. 10-fold serial dilutions were plated at the indicated time points. Experiment was performed two times with similar results; one experiment shown.

(D) and (E), 6-TreAz labeling of wild-type and Δ*sugC M. smegmatis* (*Msmeg*) and *M. tuberculosis* (*Mtb*) cultured in low or high carbon medium. Azides were detected by strain-promoted azide-alkyne cycloaddition (SPAAC) with DBCO-Cy5 label. Fluorescence was detected by flow cytometry, with median fluorescence intensity (MFI) values from controls lacking 6-TreAz (but subjected to SPAAC) subtracted from sample

MFI. Experiment was performed at least three times in triplicate; one representative experiment shown.

(F) and (G), TMM abundance in *M. smegmatis* and *M. tuberculosis* cultured in low or high carbon medium. TLCs were scanned and processed in ImageJ (99). Data are normalized to TLCs from mycobacteria cultured in high carbon medium and plotted from two (*M. tuberculosis*) or three (*M. smegmatis*) independent experiments. Representative TLCs, **Figure S3B, S3C**.

Error bars, standard deviation. Statistical significance of low vs. high carbon samples was assessed by two-tailed Student's t test. *, $p<0.05$.

Figure 3. Trehalose recycling promotes redox and energy homeostasis under carbon limitation.

(A) and (B), Sensitivity of carbon-deprived wild-type, Δ*sugC* and complemented Δ*sugC* (CΔ*sugC*) *M. smegmatis* (A) or *M. tuberculosis* (B), to hydrogen peroxide. 10-fold serial dilutions were plated. White triangles highlight most sensitive strain or condition. The sensitivity of each strain or condition was assessed at least three independent times; representative data shown.

(C) Staining of *M. smegmatis* cultured in 0.02% glucose-supplemented medium by superoxide indicator dye dihydroethidium (DHE). Fluorescence detected by flow

cytometry and median fluorescence intensity (MFI) plotted. Experiment was performed three times in triplicate; one representative experiment shown.

(D) Oxygen consumption of *M. smegmatis* cultured in 0.02% glucose-supplemented medium. Strains were incubated +/- methylene blue and absorbance at 665 nm was measured. Absorbance from untreated samples subtracted then normalized to those of wild-type. Data are plotted for three independent experiments performed in triplicate.

(E) ATP levels of *M. smegmatis* cultured in 0.02% glucose-supplemented medium. Protein concentration-normalized cell lysates were incubated with BacTiter-Glo™ reagent and luminescence was measured in relative light-forming unites (RLU). Experiment was performed at least three times in triplicate; one representative experiment shown.

(F) Cartoon summary of **Figures 3** and **S5**.

Error bars, standard deviation. Statistical significance of Δ*sugC* or complement vs. wild-type (C-E) from at least three independent experiments was assessed by two-tailed Student's t test. *, $p<0.05$.

Figure 4. Trehalose anabolism disrupts redox balance under carbon limitation.

(A) Expression of trehalose biosynthesis genes by qRT-PCR. Wild-type and Δ*sugC M. smegmatis* were cultured in 0.02% glucose-supplemented medium. Expression data were first normalized to the housekeeping gene *sigA* then plotted as a ratio of Δ*sugC* to

wild-type. Data are combined from three independent experiments performed in triplicate.

(B) Glucose-6-phosphate (G6P) levels of *M. smegmatis* cultured in 0.02% glucose-supplemented medium. Protein concentration-normalized cell lysates were incubated with G6P working solution and G6P level was measured in 96-well plate by monitoring the absorbance ratio at 575 nm/605 nm. Data are plotted for three independent experiments performed in duplicate. G6P levels normalized to those of wild-type.

(C) Sensitivity of carbon-deprived *M. smegmatis* to hydrogen peroxide upon trehalase overexpression. 10-fold serial dilutions were plated at the indicated time points. White triangles highlight the difference in sensitivity +/- *otsA*. –Tre, plasmid backbone only; +Tre, plasmid with gene encoding trehalase under acetamide-inducible promoter; Acet, acetamide. The sensitivity of each strain or condition was assessed at least three independent times; representative data shown.

Error bars, standard deviation. Statistical significance of expression in Δ*sugC* relative to wild-type, (A), or other strains vs. wild-type, (B), was assessed by two-tailed Student's t test. *, $p<0.05$; **, $p<0.005$.

Figure 5. Trehalose recycling promotes *M. tuberculosis* survival in macrophages.

(A) Survival of wild-type, Δ*sugC* and complemented Δ*sugC* (CΔ*sugC*), *M. tuberculosis* in immortalized C57BL/6 bone marrow-derived macrophages (iBMDM) +/- IFN-γ

treatment at 3 days post-infection. Experiment was performed at least three times in duplicate or triplicate; one representative experiment shown. CFU, colony-forming units.

(B) Wild-type and Δ*sugC M. tuberculosis* survival in IFN-γ-stimulated iBMDM at 0, 2 and 5 days post-infection. Log_{10}-transformed data are combined from three to seven independent experiments performed in duplicate or triplicate.

(C) Left, Survival of wild-type, Δ*sugC* and Δ*lpqY M. tuberculosis* in IFN-γ –activated iBMDM +/- bedaquiline (BDQ) or rifampicin (RIF) at 2 days post-infection. CFU from each condition were normalized to untreated wild-type. Raw data are shown in **Figure S8B**. Right, Bliss independence scores for mutant-drug interactions were obtained by subtracting the expected values for inhibition from the observed. The expected values were calculated as in Materials and Methods. Combined data from five (RIF) or six (BDQ) independent experiments.

Error bars, standard deviation. Statistical significance was assessed by two-tailed Student's t test on log_{10}-transformed data at each time point, (B), or by comparing expected and observed values for mutant-drug interactions, (C), right. *, $p<0.05$.

Figure 6. Model for the role of trehalose recycling in mycomembrane remodeling under nutrient or host stress.

Bottom, mycobacteria respond to growth-limiting carbon deprivation by turning over TDM and synthesizing AGM along the entire cell periphery. Top, in wild-type cells, the

TMM building blocks are obtained at least in part from trehalose recycled by LpqY-SugABC. In mutants unable to recycle trehalose (red X), TMM is supplied by *de novo* trehalose synthesis (dark arrow), which in turn depletes ATP, drives respiration and confers ROS sensitivity.

Supplementary Figure Legends

Figure S1. Effect(s) of carbon source and amount on *M. smegmatis* growth and cell envelope labeling.

(A) Growth of *M. smegmatis* grown in different carbon sources. Experiment was performed twice in triplicate with similar results; one experiment shown. Arrow indicates time at which cultures were labeled with O-AlkTMM or HADA.

(B) O-AlkTMM (primarily incorporates into AGM) and (C) HADA (incorporates into peptidoglycan) labeling of *M. smegmatis* cultured in medium supplemented with different carbon sources. Alkynes were detected by CuAAC reaction with carboxyrhodamine 110 azide. Data are normalized to labeling in 2% glucose-supplemented medium and plotted from three independent experiments. Cyan autofluorescence subtracted from values in (C).

Error bars, standard deviation.

Figure S2. Quantitation of mycomembrane components in high and low carbon media.

(A) Mycomembrane components extracted from *M. smegmatis* and analyzed by thin-layer chromatography (TLC). TDM, trehalose dimycolate; AGM-MA, covalently-bound mycolic acids; CS-MA, free mycolic acids from culture supernatant.

Representative TLCs of (B) TDM, (C) AGM-MA, and (D) CS-MA. Wild-type (WT) and Δ*sugC M. smegmatis* were cultured for 24 hours in 0.02% or 2% glucose-supplemented medium and processed for lipid extraction. Samples were normalized by wet pellet weight, (B), the extracted mAGP dry weight, (C), or by optical density, (D). The black boxes highlight the bands used for quantification (**Figure 1D**) and arrows denote the standards. STD, standard (purified TDM or mycolic acids).

Figure S3. Metabolic labeling and quantitation of TMM in high and low carbon media.

(A) Metabolic labeling of wild-type and Δ*sugC M. smegmatis* in 0.02% and 2% glucose-supplemented medium with 6-TreAz (labels TMM). After fixation, alkynes were detected by CuAAC reaction with carboxyrhodamine 110 alkyne. Scale bars, 10 μM.

(B) & (C) Representative images of thin-layer chromatography (TLC) of TMM from wild-type (WT), Δ*sugC* and complemented (*C*Δ*sugC*) *M. smegmatis* (B) or *M. tuberculosis* (C) cultured for 24 hours in low or high carbon medium. Samples were normalized by wet pellet weight in (B) or optical density in (C). The black boxes highlight the bands

used for quantification (**Figures 2F, 2G**) and arrows denote the standards. STD, standard (purified TMM).

Figure S4. Mycomembrane reorganization under carbon deprivation does not require trehalose recycling.

(A) Mycomembrane biosynthesis and turnover continues in the absence of trehalose recycling.

Quantitation of TMM abundance in Δ*sugC* and complemented (*C*Δ*sugC*) *M. smegmatis* (B) or *M. tuberculosis* (C) cultured for 24 hours in low carbon medium. TLCs were scanned and processed in ImageJ (99). Data were normalized to wild-type *M. smegmatis* (A) or *M. tuberculosis* (B) and plotted from three independent experiments, including images from **Figure S3B** and **S3C**.

(D) Quantitation of metabolic labeling of wild-type and Δ*sugC M. smegmatis* in 0.02% and 2% glucose-supplemented medium with O-AlkTMM (primarily labels AGM), N-AlkTMM (labels TDM) and alkDala (labels peptidoglycan). After fixation, alkynes were detected by CuAAC reaction with carboxyrhodamine 110 azide. Fluorescence was quantitated by flow cytometry and expressed as median fluorescence intensity (MFI). Experiment was performed 3 times in triplicate; one representative experiment shown.

(E) TDM turnover in Δ*sugC M. smegmatis* under carbon deprivation (compare to data for wild-type in **Figure 1B, right**). Δ*sugC M. smegmatis* was cultured in 0.02% glucose-supplemented medium in the presence of metabolic probes O-AlkTMM (primarily labels AGM), N-AlkTMM (labels TDM) or HADA (labels cell wall peptidoglycan). After 24

hours, cultures were washed and resuspended in probe-free medium. Aliquots were removed 0, 4 and 8 hours into the chase and fixed with 2% formaldehyde. Alkynes were detected by copper-catalyzed azide-alkyne cycloaddition (CuAAC) reaction with carboxyrhodamine 110 azide. Fluorescence was quantitated by flow cytometry, with the median fluorescence intensities normalized to the initial, 0 h time point for each probe. Experiment was performed three times in triplicate; one representative experiment shown.

(F) Propidium iodide staining of wild-type and Δ*sugC M. smegmatis* after 24 hours in 0.02% glucose-supplemented medium. Fluorescence was quantitated by flow cytometry and median fluorescence intensity (MFI) was plotted. Experiment was performed three times in triplicate; one representative experiment shown.

Error bars, standard deviation.

Figure S5. Trehalose recycling promotes redox balance under carbon limitation.

(A) Effect of thiourea pre-treatment on hydrogen peroxide sensitivity of of carbon-deprived Δ*sugC M. smegmatis.*

(B) Sensitivity of carbon-deprived wild-type, Δ*sugC* and complemented Δ*sugC* (CΔ*sugC*) *M. tuberculosis* to vitamin C.

For both (B) and (C), 10-fold serial dilutions were plated. White triangles highlight most sensitive strain or condition. Experiments were performed at least three times; representative data are shown.

(C) Quantification of total free thiols. Cell lysates of *M. smegmatis* that had been cultured in 0.02% glucose-supplemented medium were incubated with 5,5′-dithiobis (2-nitrobenzoic acid) and the absorbance at 412 nm was measured. Experiment was performed two times in triplicate with similar results; one experiment shown.

(D) $NADP^+$/ NADPH levels from *M. smegmatis* cultured in 0.02% glucose-supplemented medium. Ratios plotted from three independent experiments performed in triplicate.

Statistical significance of Δ*sugC* vs. wild-type NADP/NADPH ratios was assessed by two-tailed Student's t test. **, $p<0.005$.

Figure S6. Depletion of trehalose pool or inhibition of trehalose catabolism is not sufficient to cause oxidative stress.

(A) Trehalose biosynthetic pathways. Light blue, phosphorylated glucose intermediates. Purple, α-glucan polymer.

(B) Quantification of intracellular trehalose from *M. smegmatis* cultured in 0.02% glucose-supplemented medium. Data plotted from three independent experiments performed in triplicate. The obtained values for colorimetric detection of trehalose were normalized to wild-type.

(C) Staining of *M. smegmatis* cultured in 0.02% glucose-supplemented medium by superoxide indicator dye dihydroethidium (DHE). Fluorescence detected by flow cytometry and median fluorescence intensities (MFI) of the different mutants were normalized to wild-type. Data plotted from two independent experiments for complemented Δ*sugC (*CΔ*sugC*), and from four independent experiments for the rest of the strains. Experiments performed in triplicate. DHE fluorescence for all strains normalized to that of wild-type strain.

(D), (E), (F) Hydrogen peroxide sensitivity of carbon-deprived wild-type and mutant *M. smegmatis*. 10-fold serial dilutions were plated at the indicated time points. Experiments were performed 2-3 times; representative data shown. White triangles highlight most sensitive strains or conditions. –Tre, plasmid backbone pYAB-EV only; +Tre, plasmid with gene encoding trehalase (pYAB-Tre) under acetamide-inducible promoter; Acet, acetamide. Experiments were performed 2-3 times; representative data shown.

(G), (H) Quantification of intracellular trehalose from carbon-deprived wild-type and mutant *M. smegmatis*. Data in (G) are expressed as ratios of trehalose from acetamide-induced:uninduced for *M. smegmatis* expressing pYAB-EV and pYAB-Tre. Ratios plotted from three independent experiments performed in triplicate. Representative data are shown for (H).

Error bars, standard deviation. Statistical significance of mutants vs. wild-type (B-C) or +/- trehalase expression (G) was assessed by two-tailed Student's t test. *, $p<0.05$; **, $p<0.005$.

Figure S7. Trehalose recycling limits glucose metabolism.

(A) Fluorescent glucose analogue 2-(N-(7-Nitrobenz-2-oxa-1,3-diazol-4-yl)Amino)-2-Deoxyglucose (2-NBDG) was added to wild-type (WT), Δ*sugC* and complemented (*C*Δ*sugC*) *M. smegmatis* that had been cultured in 0.02% glucose-supplemented medium. Samples were normalized by wet pellet weight. Aqueous extracts were processed using the same conditions and solvent systems used to detect cytoplasmic trehalose (**Figures S6B, S6G** and **S6H**). Left TLC, fluorescent carbohydrates; right TLC, all carbohydrates. Boxed areas highlight prominent fluorescent species that were reliably enhanced in Δ*sugC* relative to wild-type or complement and arrows denote the standards. STD, standard (purified 2-NBDG or trehalose). Experiment was performed three times; representative TLCs shown.

(B) Fluorescent TLCs were scanned and processed in ImageJ (99). The intensities of the most prominent fluorescent bands were normalized to the sum of all of the fluorescent bands. Data are plotted from three independent experiments.

(C) Cartoon summary of **Figure S7A, S7B**. In the absence of trehalose recycling there is enhanced metabolism of 2-NBDG.

Error bars, standard deviation. Statistical significance of relative fluorescence intensity in wild-type vs. Δ*sugC* was assessed by two-tailed Student's t test. *, $p<0.05$.

Figure S8. Survival of trehalose recycling mutant *M. tuberculosis* in macrophages +/- IFN-γ or +/- antibiotics.

(A) Intracellular survival of Δ*sugC* in iBMDM relative to wild-type (WT) *M. tuberculosis* +/- IFN-γ at three days post-infection. Colony-forming unit (CFU) ratios plotted from three independent experiments, including data from **Figure 5A**.

(B) Survival of wild-type, Δ*sugC* and Δ*lpqY M. tuberculosis* in IFN-γ –activated iBMDM +/- bedaquiline (BDQ) or rifampicin (RIF) at 2 days post-infection. Log_{10}-transformed data are combined from five or six independent experiments performed in duplicate or triplicate. Data normalized to untreated wild-type are presented in **Figure 5C**, left.

Error bars, standard deviation. Statistical significance in assessed by two-tailed Student's t test by comparing fold change in CFU of Δ*sugC* relative to wild-type +/- IFN-γ activation, (A), or by comparing log_{10}-transformed data of mutants relative to wild-type for each condition. *, $p<0.05$.

Figure 1

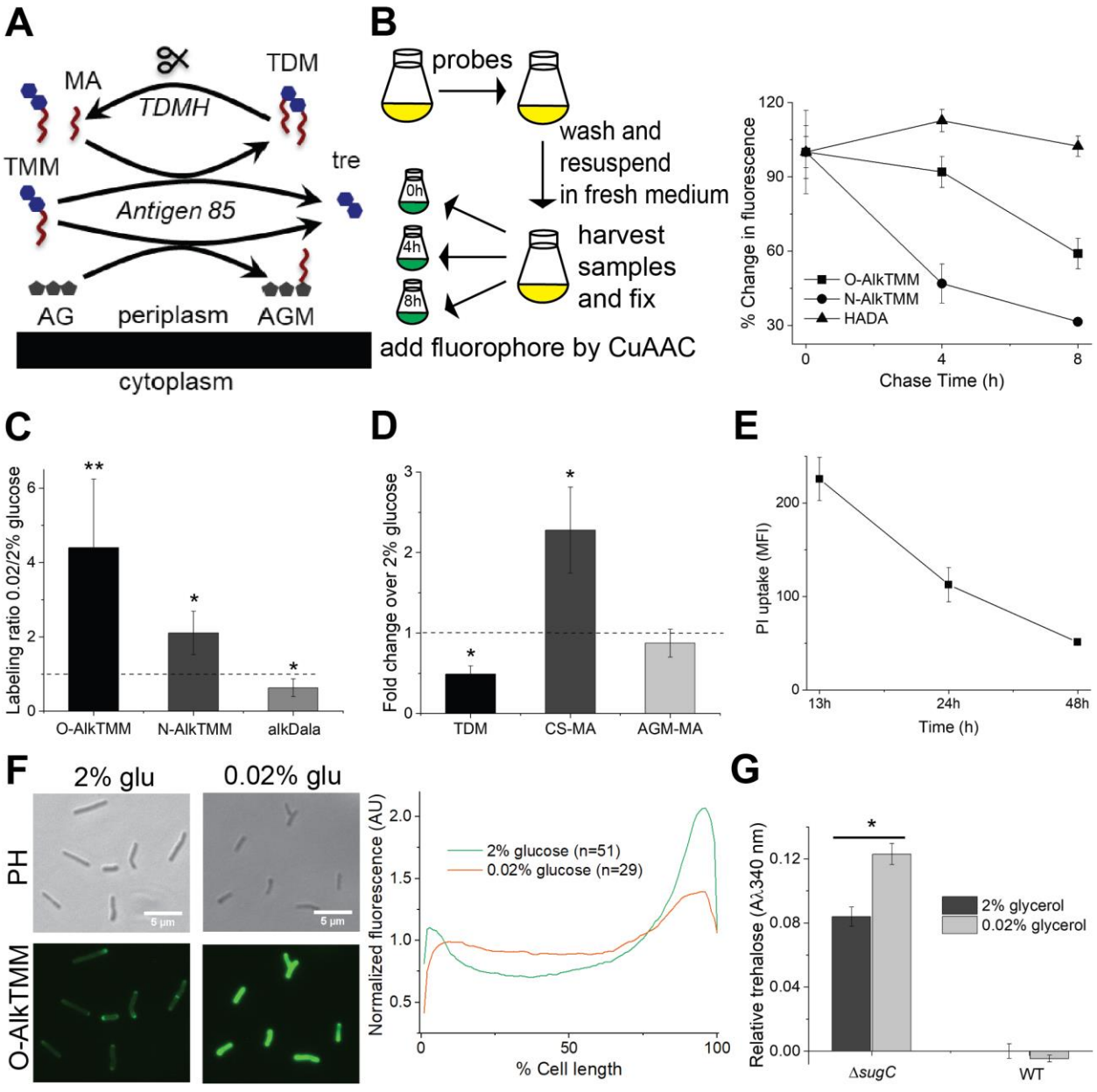
A
MA
TDM
TDMH
TMM
tre
Antigen 85
AG
periplasm
AGM
cytoplasm
B
probes
wash and
resuspend
in fresh medium
0h
4h
8h
harvest
samples
and fix
add fluorophore by CuAAC
% Change in fluorescence
O-AlkTMM
N-AlkTMM
HADA
Chase Time (h)
C
Labeling ratio 0.02/2% glucose
O-AlkTMM
N-AlkTMM
alkDala
D
Fold change over 2% glucose
TDM
CS-MA
AGM-MA
E
PI uptake (MFI)
Time (h)
F
2% glu
0.02% glu
PH
O-AlkTMM
5 µm
Normalized fluorescence (AU)
2% glucose (n=51)
0.02% glucose (n=29)
% Cell length
G
Relative trehalose (A340 nm)
2% glycerol
0.02% glycerol
ΔsugC
WT

Figure 2

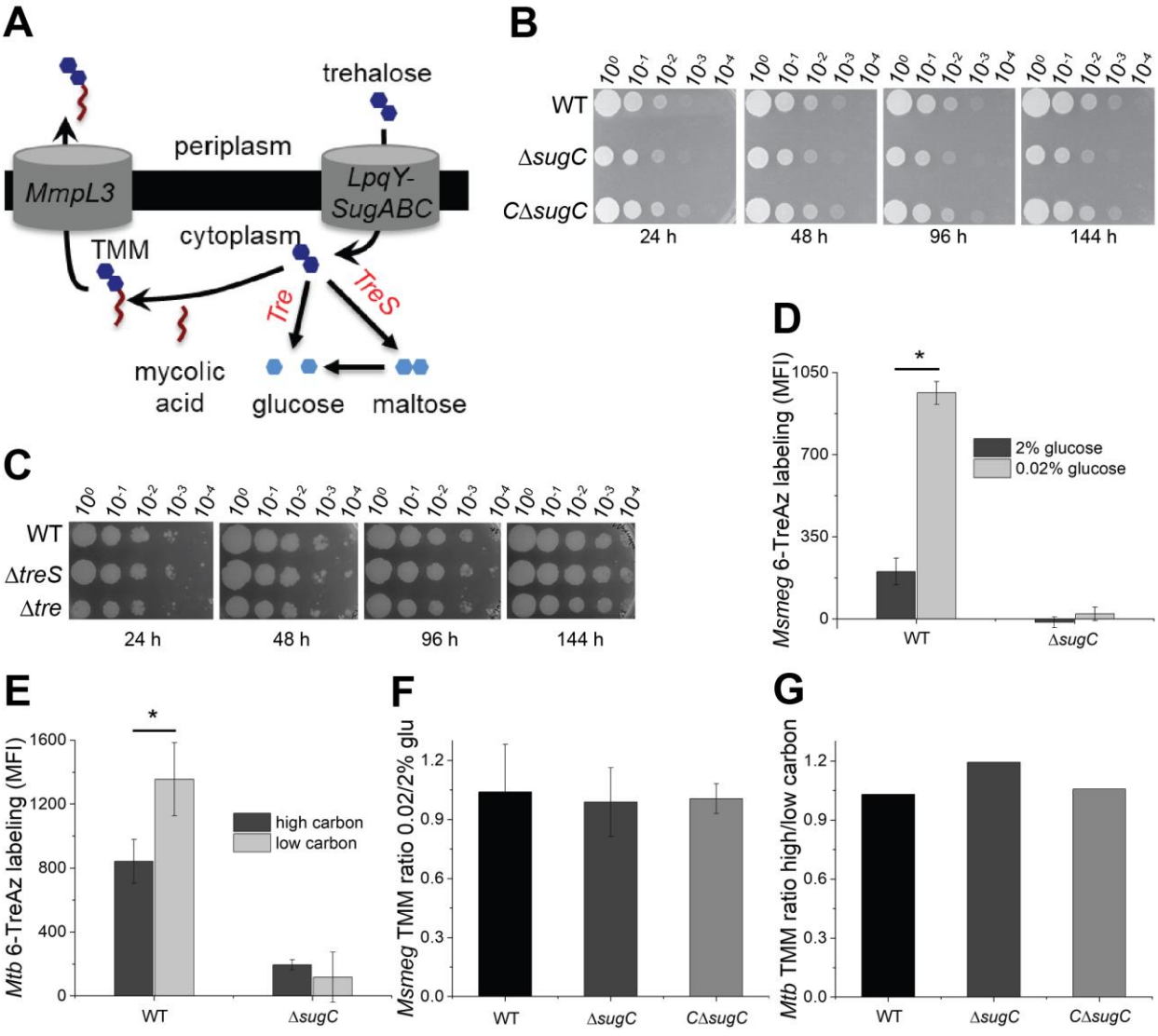
A
trehalose
periplasm
MmpL3
LpqY-SugABC
cytoplasm
TMM
Tre
TreS
mycolic acid
glucose
maltose
B
WT
ΔsugC
CΔsugC
24 h
48 h
96 h
144 h
C
WT
ΔtreS
Δtre
24 h
48 h
96 h
144 h
D
Msmeg 6-TreAz labeling (MFI)
2% glucose
0.02% glucose
WT
ΔsugC
E
Mtb 6-TreAz labeling (MFI)
high carbon
low carbon
WT
ΔsugC
F
Msmeg TMM ratio 0.02/2% glu
WT
ΔsugC
CΔsugC
G
Mtb TMM ratio high/low carbon
WT
ΔsugC
CΔsugC

1

Figure 3

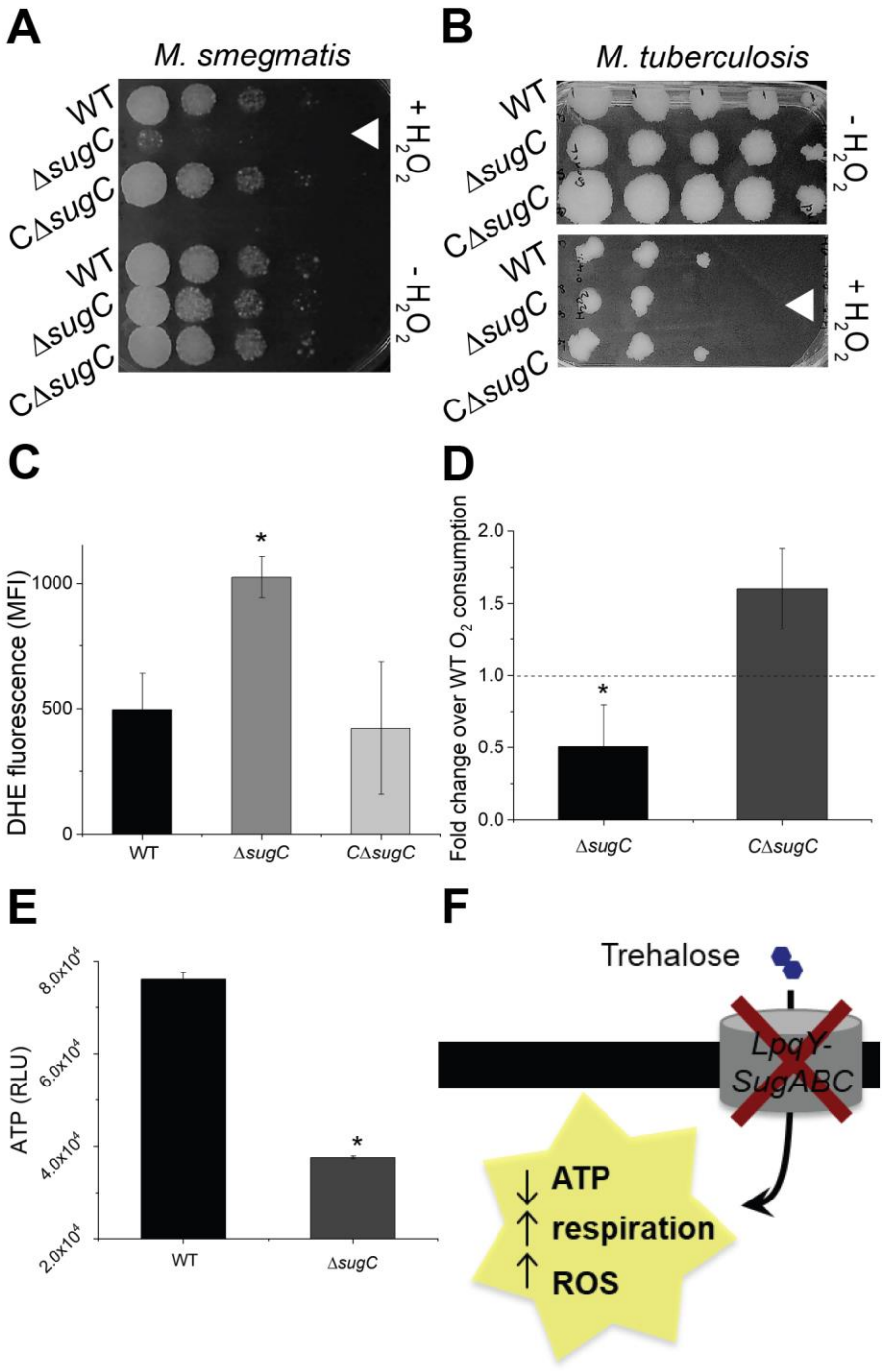
A
M. smegmatis
WT
ΔsugC
CΔsugC
WT
ΔsugC
CΔsugC
+ H2O2
- H2O2
B
M. tuberculosis
WT
ΔsugC
CΔsugC
WT
ΔsugC
CΔsugC
- H2O2
+ H2O2
C
DHE fluorescence (MFI)
1000
500
0
*
WT
ΔsugC
CΔsugC
D
Fold change over WT O2 consumption
2.0
1.5
1.0
0.5
0.0
*
ΔsugC
CΔsugC
E
ATP (RLU)
8.0x10⁴
6.0x10⁴
4.0x10⁴
2.0x10⁴
*
WT
ΔsugC
F
Trehalose
LpqY-SugABC
↓ ATP
↑ respiration
↑ ROS

1

Figure 4

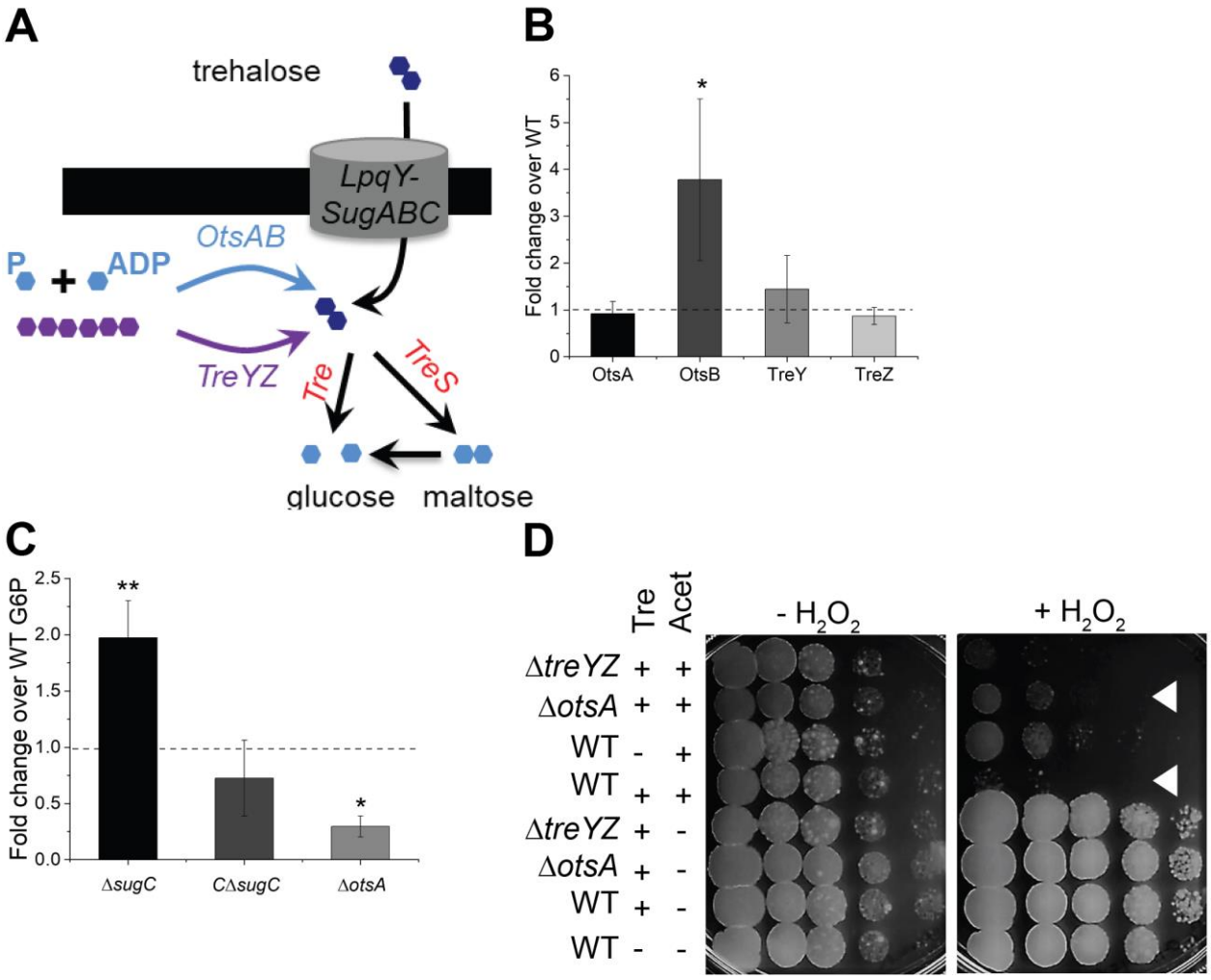
A
trehalose
LpqY-
SugABC
OtsAB
P
+
ADP
TreYZ
Tre
TreS
glucose
maltose
B
Fold change over WT
6
5
4
3
2
1
0
*
OtsA
OtsB
TreY
TreZ
C
Fold change over WT G6P
2.5
2.0
1.5
1.0
0.5
0.0
**
*
ΔsugC
CΔsugC
ΔotsA
D
Tre
Acet
- H2O2
+ H2O2
ΔtreYZ + +
ΔotsA + +
WT - +
WT + +
ΔtreYZ + -
ΔotsA + -
WT + -
WT - -

Figure 5

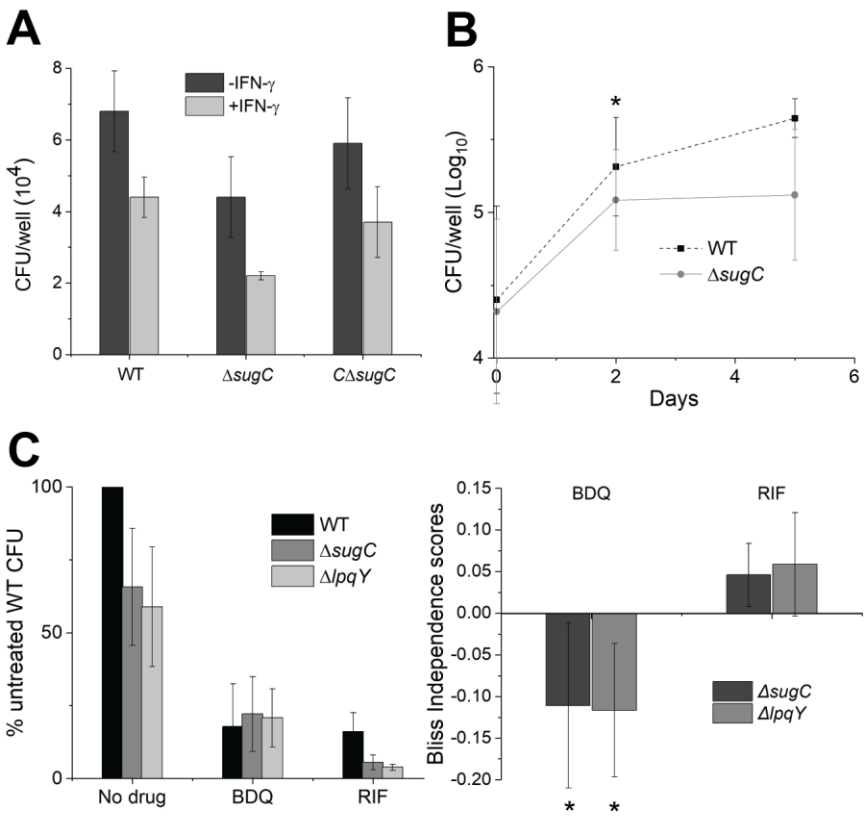
A
B
C
-IFN-γ
+IFN-γ
CFU/well (10^4)
WT
ΔsugC
CΔsugC
CFU/well (Log10)
Days
WT
ΔsugC
% untreated WT CFU
No drug
BDQ
RIF
ΔlpqY
Bliss Independence scores
BDQ
RIF
ΔsugC
ΔlpqY

1

Figure 6

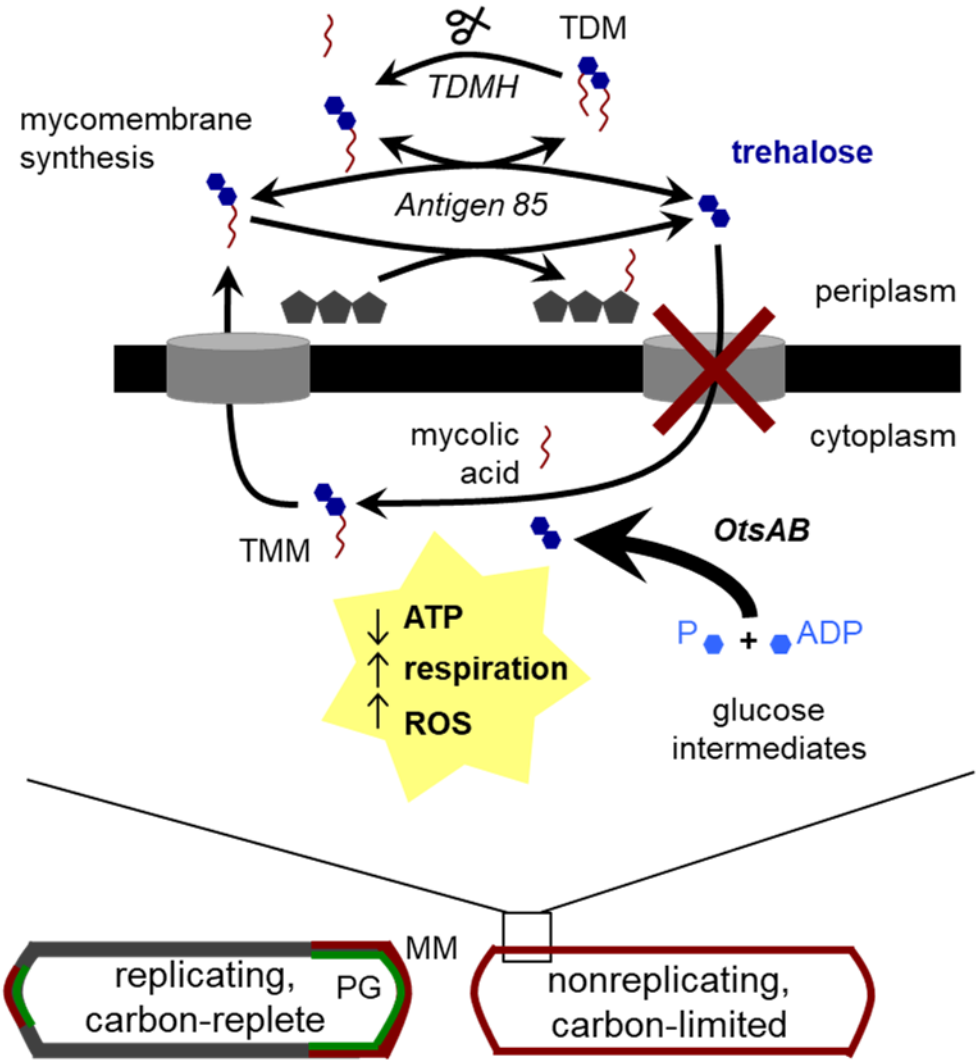
TDM
TDMH
mycomembrane
synthesis
trehalose
Antigen 85
periplasm
cytoplasm
mycolic
acid
TMM
OtsAB
ATP
respiration
ROS
P
+
ADP
glucose
intermediates
MM
replicating,
carbon-replete
PG
nonreplicating,
carbon-limited

1

2